

The VIMOS VLT Deep Survey

The contribution of minor mergers to the growth of $L_B \gtrsim L_B^*$ galaxies since $z \sim 1$ from spectroscopically identified pairs

C. López-Sanjuan^{1,*}, O. Le Fèvre¹, L. de Ravel², O. Cucciati¹, O. Ilbert¹, L. Tresse¹, S. Bardelli³, M. Bolzonella³, T. Contini⁴, B. Garilli⁵, L. Guzzo⁶, D. Maccagni⁵, H. J. McCracken^{7,8}, Y. Mellier^{7,8}, A. Pollo^{9,10,11}, D. Vergani⁵, and E. Zucca³

(Affiliations can be found after the references)

Received 28 September 2010 / Accepted 17 February 2011

ABSTRACT

Aims. The role of minor galaxy mergers in galaxy evolution, and in particular to mass assembly, is an open question. In this work we measure the merger fraction, f_m , of $L_B \gtrsim L_B^*$ galaxies in the VVDS-Deep spectroscopic survey, and study its dependence on the B -band luminosity ratio of the galaxies in the pair, $\mu \equiv L_{B,2}/L_{B,1}$, focusing on minor mergers with $1/10 \leq \mu < 1/4$, and on the rest-frame $NUV - r$ colour of the principal galaxies.

Methods. We use spectroscopic pairs with redshift $z \lesssim 1$ in the VVDS-Deep survey to define kinematical close pairs as those galaxies with a separation on the sky plane $5h^{-1}$ kpc $< r_p \leq r_p^{\max}$ and a relative velocity $\Delta v \leq 500$ km s $^{-1}$ in redshift space. We vary r_p^{\max} from $30h^{-1}$ kpc to $100h^{-1}$ kpc. We study f_m in two redshift intervals and for several values of μ , from 1/2 to 1/10.

Results. The merger fraction dependence on μ is well described by a power-law function, $f_m(\geq \mu) \propto \mu^s$. The value of s evolves from $s = -0.60 \pm 0.08$ at $z = 0.8$ to $s = -1.02 \pm 0.13$ at $z = 0.5$. The fraction of minor mergers for bright galaxies shows little evolution with redshift as a power-law $(1+z)^m$ with index $m = -0.4 \pm 0.7$ for the merger fraction and $m = -0.5 \pm 0.7$ for the merger rate, in contrast with the increase in the major merger fraction ($m = 1.3 \pm 0.5$) and rate ($m = 1.3 \pm 0.6$) for the same galaxies. We split our principal galaxies in red and blue, finding that i) f_m is higher for red galaxies at every μ , ii) f_m^{red} does not evolve with z , with $s = -0.79 \pm 0.12$ at $0.2 < z < 0.95$, and iii) f_m^{blue} evolves dramatically: the major merger fraction of blue galaxies decreases by a factor of three with cosmic time, while the minor merger fraction of blue galaxies is roughly constant.

Conclusions. Our results show that the mass of normal $L_B \gtrsim L_B^*$ galaxies has grown by about 25% since $z \sim 1$ because of mergers. The relative contribution of the mass growth by merging is $\sim 25\%$ due to minor mergers and $\sim 75\%$ due to major mergers. The relative effect of merging is more important for red than for blue galaxies, with red galaxies subject to 0.5 minor and 0.7 major mergers since $z \sim 1$, which leads to a mass growth of $\sim 40\%$ and a size increase by a factor of 2. Our results also suggest that, for blue galaxies, minor mergers likely lead to early-type spirals rather than elliptical galaxies. These results show that minor merging is a significant but not dominant mechanism contributing to the mass growth of galaxies in the last ~ 8 Gyr.

Key words. Galaxies : evolution — galaxies : formation — galaxies : interactions

1. Introduction

As galaxies evolve along cosmic time in the framework of a hierarchical assembly of dark matter haloes, a significant fraction of their accreted mass is expected to come from galaxy-galaxy mergers. The total stellar mass density is increasing along cosmic time, faster for early-type galaxies (e.g., Drory et al. 2005; Bundy et al. 2005; Arnouts et al. 2007; Ilbert et al. 2010), and galaxy-galaxy merging is a natural physical process to participate to this growth. The role of mergers in galaxy evolution

has long been recognised, leading to mass growth and perturbed morphologies, and mergers have been identified as a way to shape elliptical galaxies.

Major mergers, the encounter of two galaxies of comparable masses leading to a fusion, have now been well documented in the nearby as well as in the distant universe. While the fraction of major mergers in the nearby Universe is about 2% (Patton et al. 2000; Patton & Atfield 2008; Darg et al. 2010), it has now been convincingly shown that major mergers were more numerous at redshifts up to $z \sim 1$ (e.g., Le Fèvre et al. 2000; Patton et al. 2002; Lin et al. 2008; de Ravel et al. 2009; López-Sanjuan et al. 2009b), with the merger rate of bright/massive galaxies staying relatively stable along cosmic time, while the merger rate of intermediate luminosity/mass galaxies was stronger in the past (de Ravel et al. 2009). Major mergers have been shown to contribute a significant but not dominant part of the mass growth above the characteristic luminosity L^* , with major mergers being responsible for about 20% of the stellar mass growth (Bundy et al. 2009; Wild et al. 2009; de Ravel et al. 2009; López-Sanjuan et al. 2010b).

* Based on data obtained with the European Southern Observatory Very Large Telescope, Paranal, Chile, under Large Programs 070.A-9007 and 177.A-0837. Based on observations obtained with MegaPrime/MegaCam, a joint project of CFHT and CEA/DAPNIA, at the Canada-France-Hawaii Telescope (CFHT) which is operated by the National Research Council (NRC) of Canada, the Institut National des Sciences de l'Univers of the Centre National de la Recherche Scientifique (CNRS) of France, and the University of Hawaii. This work is based in part on data products produced at TERAPIX and the Canadian Astronomy Data Centre as part of the Canada-France-Hawaii Telescope Legacy Survey, a collaborative project of NRC and CNRS.

As major mergers are apparently not the most important contributor to the mass growth since $z \sim 1$, other processes need to have taken place. Secular processes such as steady cold accretion (Genel et al. 2010, and references therein) or other mass accretion processes like minor mergers must drive this transformation. The merging of smaller galaxies with a more massive one, the minor merger process, is a possible way to increase the mass of galaxies as minor mergers, if frequent, could lead to a significant mass increase. Indirect evidence for minor merging has been presented in the recent literature, including recent star formation in early-type galaxies being compatible with a minor merger origin (Kaviraj et al. 2007, 2009; Fernández-Ontiveros et al. 2011), as confirmed by simulations (Mihos & Hernquist 1994; Bournaud et al. 2007).

However, so far only few attempts to study the minor merger rate in the local Universe or beyond have been published. Unfortunately, to our knowledge, there are no references to the minor merger rate in local galaxies. At higher redshifts, Lotz et al. (2008) and Jogee et al. (2009) use distortions in galaxy morphologies to infer that the combined major and minor merger fraction is nearly constant since $z \sim 1$. On the other hand, López-Sanjuan et al. (2010a) estimates that the major and minor merger rate is ~ 1.7 times the major rate for $\log(M_\star/M_\odot) \geq 10$ galaxies in GOODS-S at $0.2 < z < 1.1$ from their spectro-photometric catalogue.

Here we report the results from the first measurement of the minor merger fraction and rate using kinematically confirmed close pairs. We use the VVDS-Deep spectroscopic redshift survey which offers a unique combination of deep spectroscopy ($I_{AB} \leq 24$) to identify faint merging companions, and a wide area (0.5 deg^2) which contains enough bright galaxies for a statistically robust analysis.

This paper is organized as follows. In Sect. 2 we summarize the second epoch VVDS-Deep survey data set, while in Sect. 3 the methodology and weight scheme to obtain the merger fraction by close pair statistics and its extension to the regime of minor companions. In Sect. 4 we measure the merger fraction as a function of the redshift and the luminosity ratio between the galaxies in pairs, while in Sect. 5 we study the merger fraction of red and blue galaxies. We estimate the minor merger rate of bright galaxies in Sect. 6, and we discuss the implications of our results in Sect. 7. Finally, we present our conclusion in Sect. 8. We use $H_0 = 100h \text{ km s}^{-1} \text{ Mpc}^{-1}$, $h = 0.7$, $\Omega_M = 0.3$, and $\Omega_\Lambda = 0.7$ throughout. All reported magnitudes are AB.

2. VVDS-Deep sample

The VVDS-Deep sample¹ (Le Fèvre et al. 2005b) is magnitude selected with $17.5 \leq I_{AB} \leq 24$. The spectroscopic survey has been conducted on the 0224-04 field with the VIMOS multi-slit spectrograph on the VLT (Le Fèvre et al. 2003), with 4h integration using the LRRED grism at a spectral resolution $R \sim 230$. The multi-slit data processing has been performed using the VIPGI package (Scudeggio et al. 2005). Redshift measurement has followed a strict approach, with initial guesses based on cross-correlation with reference templates at the same redshift, followed by careful eye-checking independently by two team members before confronting their results. The final redshifts and quality flags follow a statistically well defined behaviour, leading to a survey for which at least 80% of the sample has a secure redshift. This comprises sources with quality flag = 4 (99% secure), 3 (95% secure), 2 (80% secure) and 9 (those with only a

single secure spectral feature in emission in their spectrum). The accuracy in the redshift measurement is 276 km s^{-1} .

Deep photometry is available in this field from a first campaign with the CFH12K camera (Le Fèvre et al. 2004 and McCracken et al. 2003), followed by very deep observations with the CFHTLS survey. Using photometric redshifts (Ilbert et al. 2006), we show that for the galaxies making up the 20% incompleteness, about 10% have a tentative (quality flag = 1) spectroscopic redshift which is right for 50% of them, the other 10% have wrong or unknown spectroscopic redshifts, but we use photometric redshift estimates to fully understand the survey completeness as a function of magnitude, type, and redshift.

A total of 8359 galaxies with $0 < z_{\text{spec}} \leq 1.2$ and $17.5 \leq I_{AB} \leq 24$ (primary objects with flags = 1,2,3,4,9; and secondary objects, those that lie by chance in the slits, with flags = 21, 22, 23, 24, 29) from second epoch VVDS-Deep data (Le Fèvre et al., in prep.) have been used in this paper. Note that we have used flag = 1 sources, which are 50% secure and that have not been used in previous VVDS-Deep works, thanks to the improved weighting scheme in VVDS-Deep (see Sect. 3.1, for details).

3. Statistics of minor close companions in spectroscopic samples

In this section we review the commonly used methodology for computing major merger fractions by close pair statistics in spectroscopic samples, and we extend it to search for minor (i.e., faint) companions in the VVDS-Deep.

The distance between two sources can be measured as a function of their projected separation, $r_p = \theta d_A(z_i)$, and their rest-frame relative velocity along the line of sight, $\Delta v = c|z_j - z_i|/(1 + z_i)$, where z_i and z_j are the redshift of the principal (more luminous galaxy in the pair) and the companion galaxy, respectively; θ is the angular separation, in arcsec, of the two galaxies on the sky plane; and $d_A(z)$ is the angular scale, in kpc/arcsec, at redshift z . Two galaxies are defined as a close pair if $r_p^{\min} < r_p \leq r_p^{\max}$ and $\Delta v \leq \Delta v^{\max}$. The inner limit in r_p is imposed to avoid spatial resolution limitations due to the size of the observed point spread function. Reasonable limits for ground-based data are $r_p^{\min} = 5h^{-1} \text{ kpc}$, $r_p^{\max} = 20h^{-1} \text{ kpc}$, and $\Delta v^{\max} = 500 \text{ km s}^{-1}$. With these constraints, it is expected that 50%-70% of the selected close pairs will finally merge (Patton et al. 2000; Patton & Atfield 2008; Lin et al. 2004, 2010; Bell et al. 2006). We used $\Delta v^{\max} = 500 \text{ km s}^{-1}$, $r_p^{\min} = 5h^{-1} \text{ kpc}$, and varied the value of r_p^{\max} from $30h^{-1} \text{ kpc}$ to $100h^{-1} \text{ kpc}$ to study the dependence of the merger fraction with the surrounding volume.

We select principal galaxies as defined below and we look for companion galaxies that fulfill the close pair criterion for each galaxy of the principal sample. If one principal galaxy has more than one close companion, we take each possible pair separately (i.e., for the close galaxies A,B, and C, we study the pairs A-B, B-C, and A-C as independent). In addition, we impose a rest-frame B -band luminosity difference between the pair members. We denote the ratio between the luminosity of the principal galaxy, $L_{B,1}$, and the companion galaxy, $L_{B,2}$, as

$$\mu \equiv \frac{L_{B,2}}{L_{B,1}}, \quad (1)$$

and looked for those systems with $L_{B,2} \geq \mu L_{B,1}$ or, equivalently, $M_{B,2} - M_{B,1} \leq \Delta M_B = -2.5 \log \mu$, where $M_{B,1}$ and $M_{B,2}$ are the B -band absolute magnitudes of the principal and companion

¹ <http://www.oamp.fr/virmos/vvds.htm>

galaxy in the pair, respectively. We define as major companions those close pairs with $\mu \geq 1/4$, while minor companions those with $1/10 \leq \mu < 1/4$.

We aimed to reach the minor companion regime, i.e., $\mu = 1/10$ ($\Delta M_B = 2.5$). For this, we define our principal galaxy sample and companions, and redshift ranges, to preserve statistical robustness and to minimize completeness corrections (see next section). We select as principal galaxies those with $M_B^e \leq -20 \sim M_B^*$ (e.g., Ilbert et al. 2005), where $M_B^e = M_B + Qz$ and the constant $Q = 1.1$ accounts for the evolution of the luminosity function in VVDS-Deep survey (Ilbert et al. 2005). With this limit, companions with μ down to $1/10$ will be included in the VVDS-Deep sample (Fig. 1). Thanks to the wide area of VVDS-Deep, we have 1011 principal galaxies at $0.1 < z < 1.0$. To study minor companions we define as companion galaxies those with $M_B^e \leq -17.5$, and impose different luminosity ratios, $\mu \geq 1/2, 1/3, 1/4, 1/5, 1/6, 1/7, 1/8$, and $1/10$ ($\Delta M_B = 0.75, 1.2, 1.5, 1.75, 1.95, 2.1, 2.25$, and 2.5 , respectively). We define two redshift bins, named $z_{r,1} = [0.2, 0.65]$ and $z_{r,2} = [0.65, 0.95]$. In these bins, the mean redshifts of the principal galaxies, weighted to take into account their spectroscopic completeness (see next section for details), are $\bar{z}_{r,1} = 0.5$ and $\bar{z}_{r,2} = 0.8$. In the former we are complete for $\mu \geq 1/10$ companions, while in the latter we reach $\mu \geq 1/5$ (Fig. 1), therefore requiring a completeness correction for $1/10 \leq \mu < 1/5$ companions (Sect. 3.1). We are able to reach this faint companions regime due to the depth of the VVDS-Deep spectroscopy ($I_{AB} \leq 24$). The number of principal galaxies is $n_1 = 351$ at $z_{r,1}$ and $n_2 = 544$ at $z_{r,2}$, this is, $n_2/n_1 = 1.55$. On the other hand, the ratio between the probed cosmological volumes is $V_2/V_1 = 1.52$, so the number density of principal galaxies is similar in both ranges. Using the group catalog from the VVDS-Deep second-epoch data presented in Cucciati et al. (2010)² we find that 14%/13% of principal galaxies at $z_{r,1}/z_{r,2}$ are in a group with three or more members. Hence, also the environment of our principal galaxies is similar in both ranges under study.

If we find N_p close pairs in our sample for a given luminosity ratio μ , the merger fraction is

$$f_m(\geq \mu) = \frac{N_p(\geq \mu)}{N_1}, \quad (2)$$

where N_1 is the number of galaxies in the principal sample. With this definition the merger fraction is cumulative when μ decrease. This simple definition is valid for volume-limited samples, while we work with spectroscopic, luminosity-limited samples. Because of this, we must take into account the different selection effects in our measurement of the merger fraction.

3.1. Accounting for selection effects

Following de Ravel et al. (2009), we correct for three basic selection effects:

1. the limiting magnitude $I_{AB} = 24$ which imposes a loss of faint companions.
2. the spatial sampling rate and the spectroscopic success rate in measuring redshifts.
3. the loss of pairs at small separations because of the ground based seeing limitation of the observations.

² We did not use galaxies with flag = 1 and 21 in groups determination. However, only 2% of the principal galaxies have flag = 1 or 21 because they are bright.

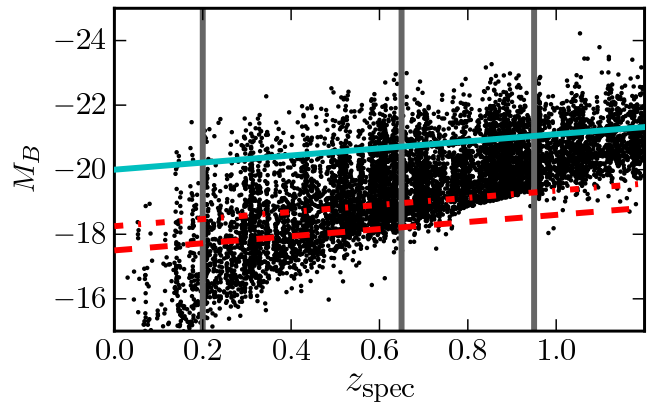


Fig. 1. B -band absolute magnitude versus redshift for all the VVDS-Deep sources with $z_{\text{spec}} \leq 1.2$. Vertical solid lines identify the redshift intervals in our study, named $z_{r,1} = [0.2, 0.65]$ and $z_{r,2} = [0.65, 0.95]$. The horizontal solid line represents the selection of the principal galaxies sample, $M_{B,1} \leq -20 - 1.1z$. The dashed line shows the limit of the companion sample down to $\mu \geq 1/10$, $M_{B,2} \leq -17.5 - 1.1z$, while the dash-dotted line shows that we are complete in both redshift bins when we search for $\mu \geq 1/5$ companions, $M_{B,2} \leq -18.25 - 1.1z$. [A colour version of this plot is available at the electronic edition].

The spectroscopic targets have been selected on the basis of the magnitude criterion $17.5 \leq I_{AB} \leq 24$. Therefore, we miss companions of the principal galaxies which have an absolute magnitude fainter than imposed by the $I_{AB} = 24$ cut off and the ΔM_B magnitude difference, artificially lowering the number of pairs. To take this into account we compute for each observed pair a weight $w_{\text{mag}}^k(M_{B,1}, z)$ using the ratio between the co-moving number densities above and below the magnitude cut off (Patton et al. 2000):

$$w_{\text{mag}}^k(M_{B,1}, z) = \frac{\int_{-\infty}^{M_{B,\text{sup}}^k} \Phi(M_B, z) dM_B}{\int_{-\infty}^{M_{B,\text{lim}}(z)} \Phi(M_B, z) dM_B}, \quad (3)$$

where $M_{B,\text{lim}}(z)$ is the limiting magnitude of the catalogue at redshift z , $M_{B,\text{sup}}^k = M_{B,1} + \Delta M_B$ is the lower luminosity of a close companion of the principal galaxy in the pair k , and $\Phi(M_B, z)$ is the luminosity function in the B -band at redshift z . We assumed the luminosity function measured in the VVDS-Deep area by Ilbert et al. (2005, see also Zucca et al. 2006). We take $w_{\text{mag}}^k = 1$ when $M_{B,\text{sup}}^k \leq M_{B,\text{lim}}(z)$. We note that the number of companions with $\mu \geq 1/10$ is complete for all principal sources with $M_B^e \leq -20$ at $z_{r,1}$ and $\sim 50\%$ at $z_{r,2}$ (Fig. 1), while the completeness is $\sim 70\%$, 80% , 90% and 100% at $z_{r,2}$ for companions with $\mu \geq 1/8, 1/7, 1/6$ and $1/5$, respectively. That is, $w_{\text{mag}}^k \neq 1$ only for $1/10 \leq \mu < 1/5$ companions of some systems at $0.65 \leq z < 0.95$. We further test the weights w_{mag}^k in Sect. 4.

Since $\sim 25\%$ of the total number of potential targets in the VVDS-Deep field have been spectroscopically observed and the redshifts are not measured with 100% certainty, we must correct for the VVDS-Deep target sampling rate and redshift success rate. These have been well constrained resulting in the Target Sampling Rate (TSR) and the Spectroscopic Success Rate (SSR) computed as a function of redshift, source magnitude and source size (x). The SSR has been assumed independent of the galaxy type, as demonstrated up to $z \sim 1$ in Zucca et al. (2006). As several first epoch VVDS-Deep galaxies with flag 1 and 2 have

been re-observed in the VVDS-Ultradeep survey ($I_{AB} \leq 24.75$, Le Fèvre et al., in prep.), providing a robust measurement of their redshift, this offers the opportunity to estimate the reliability of VVDS-Deep flag = 1 and 2 sources, and we define a weight w_{129} to take this into account. We also define the weight w_{129} for flag = 9 sources by comparison with the latest photometric redshifts in the VVDS-Deep field (see Cucciati et al. 2010, for details about the latest photometric data set in this field). By definition, $w_{129} = 1$ for flag = 3 and 4 sources. We derived the spectroscopic completeness weight for each galaxy i in the catalogue as

$$w_{\text{spec}}^i(z, I_{AB}, x) = \frac{1}{TSR^i \times SSR^i \times w_{129}^i}, \quad (4)$$

and assigned a weight $w_{\text{spec}}^k = w_{\text{spec}}^1 \times w_{\text{spec}}^2$ at each close pair, where w_{spec}^1 and w_{spec}^2 are the spectroscopic completeness weights of the principal and the companion galaxy in the pair, respectively.

The last correction we need to apply results from the observations which have been performed under a typical ground based seeing of $1''$. We correct for the increasing incompleteness in targeting both components of close pairs as the separation between them is getting smaller. Assuming a clustered distribution of galaxies, the number of galaxy pairs should be a monotonically decreasing function of the pair separation (e.g., Bell et al. 2006; Lin et al. 2008). However, pairs start to be under-counted for separations $\theta \leq 2''$ because of seeing effects. We apply a weight w_θ^k on each pair using the ratio

$$w_\theta^k = \frac{a}{r_{zz}(\theta_k)}, \quad (5)$$

where the mean ratio a is the probability to randomly select a pair, obtained at large separations, and $r_{zz}(\theta_k)$ is the ratio between the observed pair count in the spectroscopic catalogue, N_{zz} , over the observed pair count in the photometric one, N_{pp} . For large separations ($\theta > 50''$), $r_{zz} \sim a$, but at small separations $r_{zz} < a$ because of the artificial decrease of pairs due to seeing effects (see de Ravel et al. 2009, for further details). This weight also accounts for other geometrical biases in the survey, e.g., those related with the minimum separation between slits. Compared to the weight w_θ^k for the total major merger population (de Ravel et al. 2009), the weight for faint companions could be different as it is more difficult to measure the z_{spec} of fainter galaxies located near a bright principal galaxy. To explore this possibility, we compare the number of photometric and spectroscopic pairs for a given angular distance and luminosity difference in the I_{AB} band between the pair members (ΔI_{AB}). We study the variation of $r_{zz}(\theta_k, \Delta I_{AB})$ from $\theta = 1''$ to $100''$ for four different luminosity differences, $0.75 \leq \Delta I_{AB} \leq 1.5$, $1.5 < \Delta I_{AB} \leq 2$, and $2 < \Delta I_{AB} \leq 2.5$. We find that in all cases r_{zz} tends to become constant at large angular separations, while at $\theta \lesssim 10''$ the value of r_{zz} tends to be lower for higher ΔI_{AB} , making it more difficult to recover a faint companion than a bright one. However, when compared with the global value of r_{zz} , this systematic effect leads to differences $\lesssim 5\%$. Because the dispersion in the global w_θ^k is $\sim 10\%$, we have decided not to apply any correction to this systematic effect.

Finally, the corrected merger fraction is

$$f_m(\geq \mu) = \frac{\sum_{k=1}^{N_p(\geq \mu)} w_{\text{spec}}^k w_{\text{mag}}^k w_\theta^k}{\sum_i w_{\text{spec}}^i}. \quad (6)$$

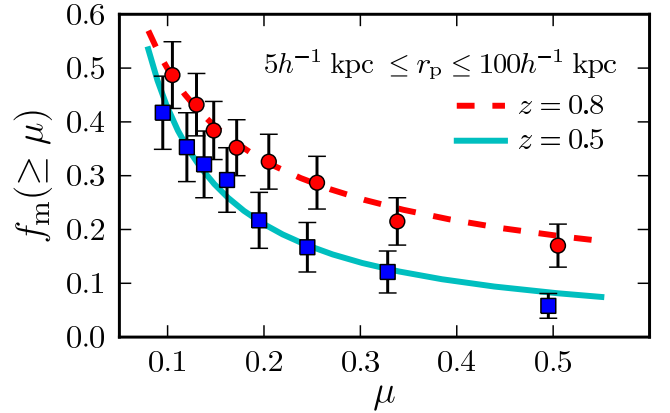


Fig. 2. Merger fraction versus luminosity ratio in B -band, μ , for close pairs with $r_p^{\min} = 5h^{-1}$ kpc and $r_p^{\max} = 100h^{-1}$ kpc. Dots are the merger fractions at $z = 0.8$, and squares at $z = 0.5$. The lines are the GLS fits of a power-law, $f_m(\geq \mu) \propto \mu^s$, to the $z = 0.8$ ($s = -0.60$; dashed) and $z = 0.5$ data ($s = -1.02$; solid). [A colour version of this plot is available at the electronic edition].

Table 1. Merger fraction of $L_{B,1} \gtrsim L_B^*$ galaxies for $r_p^{\max} = 100h^{-1}$ kpc as a function of luminosity ratio μ .

μ	$z = 0.5$		$z = 0.8$	
	$N_p(\geq \mu)$	$f_m(\geq \mu)$	$N_p(\geq \mu)$	$f_m(\geq \mu)$
1/2	6	0.058 ± 0.023	22	0.169 ± 0.040
1/3	11	0.121 ± 0.039	29	0.215 ± 0.043
1/4	15	0.167 ± 0.046	39	0.287 ± 0.049
1/5	20	0.216 ± 0.051	45	0.322 ± 0.050
1/6	26	0.291 ± 0.060	49	0.347 ± 0.052
1/7	29	0.320 ± 0.062	53	0.379 ± 0.054
1/8	33	0.351 ± 0.064	58	0.426 ± 0.057
1/10	40	0.413 ± 0.067	63	0.479 ± 0.061

In order to estimate the error of f_m we used the jackknife technique (Efron 1982). We computed partial standard deviations, δ_k , for each system k by taking the difference between the measured f_m and the same quantity with the k th pair removed for the sample, f_m^k , such that $\delta_k = f_m - f_m^k$. For a sample with N_p systems, the variance is given by $\sigma_{f_m}^2 = [(N_p - 1) \sum_k \delta_k^2]/N_p$. We checked that the variances estimated by jackknife technique are similar, within $\sim 10\%$, to those estimated by a Bayesian approach (Cameron 2010).

4. The minor merger fraction of $L_B \gtrsim L_B^*$ galaxies

In this section we study the merger fraction of bright galaxies as a function of μ , reaching the minor companion regime ($1/10 \leq \mu < 1/4$) with spectroscopically confirmed close pairs. We summarize the values of $f_m(\geq \mu)$ obtained at $z_{r,1} = [0.2, 0.65]$ and $z_{r,2} = [0.65, 0.95]$ for $r_p^{\max} = 100h^{-1}$ kpc and different luminosity ratios in Table 1, and show them in Fig. 2. The merger fraction decreases with cosmic time for all μ , but this difference is lower for smaller μ values. The merger fraction at both redshift bins increases when μ decreases, a natural consequence of our $f_m(\geq \mu)$ definition as the fraction of principal galaxies with a $L_{B,2} \geq \mu L_{B,1}$ companion.

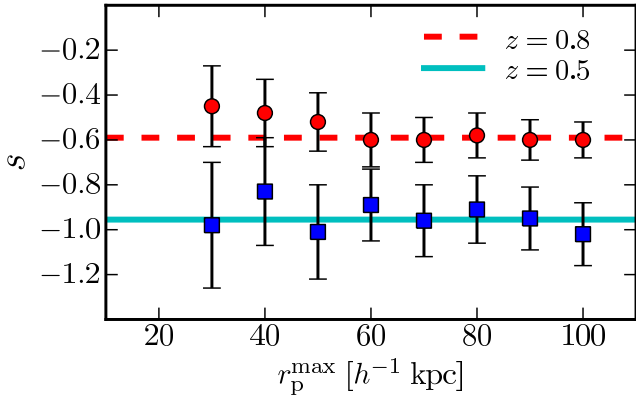


Fig. 3. Power-law index s versus r_p^{\max} . Dots are for $z = 0.8$ galaxies, and squares for $z = 0.5$ galaxies. The lines are the median of the data: $s = -0.59$ at $z = 0.8$ (dashed) and $s = -0.96$ at $z = 0.5$ (solid). [A colour version of this plot is available at the electronic edition].

Table 2. Power-law index s as a function of search radius r_p^{\max}

r_p^{\max} (h^{-1} kpc)	$z = 0.5$	$z = 0.8$
30	-0.98 ± 0.28	-0.45 ± 0.18
40	-0.83 ± 0.24	-0.48 ± 0.15
50	-1.01 ± 0.21	-0.52 ± 0.13
60	-0.89 ± 0.16	-0.60 ± 0.12
70	-0.96 ± 0.16	-0.60 ± 0.10
80	-0.91 ± 0.15	-0.58 ± 0.10
90	-0.95 ± 0.14	-0.60 ± 0.09
100	-1.02 ± 0.14	-0.60 ± 0.08

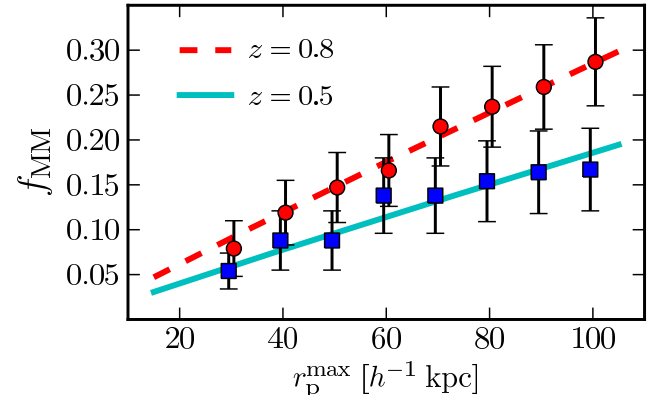


Fig. 4. Major merger fraction, f_{MM} , versus r_p^{\max} . Dots are for $z = 0.8$ galaxies, and squares for $z = 0.5$ galaxies. The lines are the least-squares best fit of a power-law function, $f_{\text{MM}} \propto r_p^q$, to the data. In both cases the power-law index is $q = 0.95$. The points are shifted to avoid overlap. [A colour version of this plot is available at the electronic edition].

Table 3. Major merger fraction of $L_{B,1} \gtrsim L_B^*$ galaxies, f_{MM} , as a function of search radius r_p^{\max}

r_p^{\max} (h^{-1} kpc)	$z = 0.5$	$z = 0.8$
30	0.054 ± 0.020	0.079 ± 0.031
40	0.088 ± 0.033	0.110 ± 0.036
50	0.088 ± 0.033	0.147 ± 0.039
60	0.138 ± 0.042	0.166 ± 0.040
70	0.138 ± 0.042	0.215 ± 0.044
80	0.154 ± 0.045	0.237 ± 0.045
90	0.164 ± 0.046	0.259 ± 0.047
100	0.167 ± 0.046	0.287 ± 0.049

The observed dependence of f_m on μ is well parametrized as

$$f_m(\geq \mu) = f_{\text{MM}} \left(\frac{\mu}{\mu_{\text{MM}}} \right)^s, \quad (7)$$

where f_{MM} is the major merger fraction ($\mu \geq \mu_{\text{MM}} = 1/4$). This dependence was predicted by the cosmological simulations of Maller et al. (2006) and used by López-Sanjuan et al. (2010a) in mass-selected spectro-photometric close pairs. We set the value of f_{MM} to the observed one and used Generalized Least Squares (GLS) to estimate the power-law index s (see Appendix A, for details). The GLS fit to the Table 1 data yields $s = -0.60 \pm 0.08$ at $z = 0.8$ and $s = -1.02 \pm 0.13$ at $z = 0.5$. To obtain a robust value of s at each redshift range under study, we determine s for different r_p^{\max} . We summarize our results in Table 2 and show them in Fig. 3. The values of s measured at $r_p^{\max} = 100h^{-1}$ are representative of the median of all the values at different r_p^{\max} , that are $s = -0.59$ at $z = 0.8$ and $s = -0.96$ at $z = 0.5$.

We find that the value of s decreases with cosmic time, reflecting a differential evolution in the merger fraction of major and minor companions. We checked that our incompleteness in the range $z_{r,2}$ (Sect. 3) does not bias our results with the following test. We define a companion sample with $M_B \leq -17.17 - 2.8z$. This sample becomes artificially incomplete for companions with $\mu \geq 1/10$ and $\mu \geq 1/5$ at $z \geq 0.2$ and $z \geq 0.65$, respectively; that is, in our first redshift bin, and mimic the completeness behaviour of our companion sample at $z_{r,2}$. Then, we

repeat the previous analysis with the artificially incomplete sample, obtaining $s = -0.99 \pm 0.08$, which is similar to the original value measured in the complete sample. This implies that the weights w_{mag}^k properly account for the missing faint companions and that the observed evolution of the index s with redshift in VVDS-Deep is a robust result. We also study how the luminosity function assumed in w_{mag}^k determination affects the measured merger fractions. We used the B -band luminosity functions from Giallongo et al. (2005); Faber et al. (2007); and Zucca et al. (2009), finding a variation lower than 3% in the values of the merger fraction for every r_p^{\max} compared to our results. Hence, assuming a different luminosity function would have only a limited impact on our results.

We then studied the dependency of the major merger fraction, f_{MM} , on the search radius. We summarize the f_{MM} values for all r_p^{\max} under study in Table 3 and show them in Fig. 4. The value of f_{MM} increases with the search radius and is well described in both redshift ranges by a power-law with index $q = 0.95 \pm 0.20$. Regarding redshift evolution, the major merger fraction increases with redshift, in agreement with previous results in the literature (e.g., Le Fèvre et al. 2000; Conselice 2006; Rawat et al. 2008; de Ravel et al. 2009; López-Sanjuan et al. 2009a,b). We study this evolution in more details in Sect. 7.1.

Table 4. Minor merger fraction, f_m ($1/10 \leq \mu < 1/4$), of $L_{B,1} \gtrsim L_B^*$ galaxies

r_p^{\max} (h^{-1} kpc)	$z = 0.5$	$z = 0.8$
30	0.084 ± 0.035	0.058 ± 0.025
50	0.136 ± 0.057	0.107 ± 0.034
100	0.259 ± 0.087	0.209 ± 0.052

We can estimate the minor-to-major merger fraction ratio, denoted $f_{m/M}$, as

$$f_{m/M} \equiv \frac{f_{\text{mm}}}{f_{\text{MM}}} = \frac{f_m(\mu_{\text{mm}} \leq \mu < \mu_{\text{MM}})}{f_m(\mu \geq \mu_{\text{MM}})} = \left(\frac{\mu_{\text{mm}}}{\mu_{\text{MM}}} \right)^s - 1, \quad (8)$$

where μ_{MM} and μ_{mm} are the luminosity ratios for major and minor mergers, respectively. This definition does not depend on the normalization of the merger fraction, that varies with r_p^{\max} (Fig. 4). We assume $\mu_{\text{MM}} = 1/4$ and $\mu_{\text{mm}} = 1/10$. We find that $f_{m/M} = 0.73 \pm 0.13$ at $z = 0.8$, and $f_{m/M} = 1.55 \pm 0.30$ at $z = 0.5$. Therefore, minor companions become more numerous than major ones as one is going to lower redshifts. To illustrate this, and to facilitate future comparisons, we summarize our best estimation of the minor merger fraction for $r_p^{\max} = 30h^{-1}$, $50h^{-1}$, and $100h^{-1}$ kpc in Table 4, and show the minor, major and total (major + minor) merger fractions for $r_p^{\max} = 100h^{-1}$ kpc in Fig. 5. The typical error in the minor merger fraction is $\sim 30 - 40\%$. Our measurements seem to indicate that the minor merger fraction increases with cosmic time. This trend becomes more robust when we further compare our results to a local ($z \sim 0.1$) estimation of the minor merger fraction, Sect. 7.1.

5. The minor merger fraction of red and blue galaxies

In this section we study the merger fraction as a function of the blue or red colour of the principal galaxy in the pair. To split our $M_B^c \leq -20$ galaxies into red and blue, we study their distribution in the $M_{NUV} - M_r$ versus $M_r - M_J$ plane. The UV – optical colours is a better tracer of recent star formation than typical optical – optical colours (Wyder et al. 2007; Schiminovich et al. 2007; Arnouts et al. 2007; Kaviraj et al. 2007), while the addition of an optical – infrared colour to the UV – optical helps to break the degeneracy between old and dusty star-forming (SF) red galaxies (Williams et al. 2009; Ilbert et al. 2010). Another possibility to separate old and dusty red galaxies is to perform a dust reddening correction. This also makes possible a clean separation between the red quiescent sequence and the blue star-forming cloud, since the “green valley” region between both sequences is mainly populated by dusty SF galaxies (Wyder et al. 2007; Cortese et al. 2008; Salim et al. 2009; Brammer et al. 2009).

In Fig. 6, we show the number density contours of $M_B^c \leq -20$ galaxies in the $M_{NUV} - M_r$ versus $M_r - M_J$ plane for the two redshift ranges under study, $z_{r,1} = [0.2, 0.65]$ and $z_{r,2} = [0.65, 0.95]$. We only show those galaxies detected in the K band to avoid that M_J was an extrapolation from the fit to the optical photometry. We find a red sequence and a blue cloud in both redshift ranges, as expected from previous works (e.g., Arnouts et al. 2007; Franzetti et al. 2007). Both populations are well separated using a constant cut $M_{NUV} - M_r = 4.25$. Because

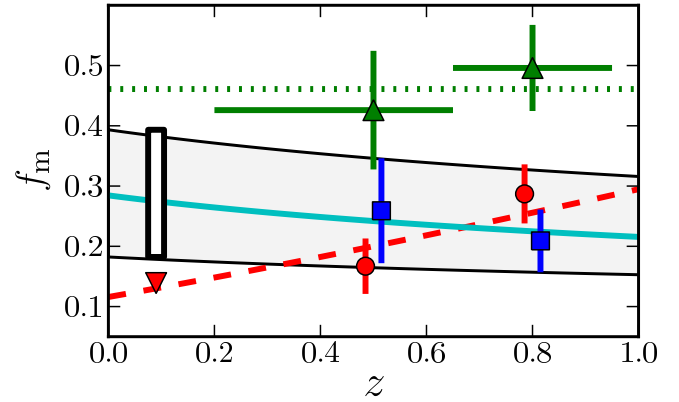


Fig. 5. Minor (squares), major (dots), and major + minor (triangles) merger fraction of $M_B^c \leq -20$ galaxies for $r_p^{\max} = 100h^{-1}$ kpc as a function of redshift. The points are shifted when necessary to avoid overlap. The z error bars in the total merger fraction mark the redshift range spanned by VVDS-Deep data. The inverted triangle is the major merger fraction at $z = 0.09$ from MGC. The white rectangle is the local ($z = 0.09$) minor merger fraction derived from the total and the major merger ones, while the gray area identifies the most probable minor merger fraction values in the range $0 < z < 1$ (see text for details). The solid line is the best fit of a power-law function with a fixed index, $f_{\text{mm}} \propto (1+z)^{-0.4}$, to the minor merger fraction data. The dashed line is the least-squares best fit of a power-law function to the major merger fraction data. The dotted line is the major + minor merger fraction if it is assumed constant. [A colour version of this plot is available at the electronic edition].

of our rest-frame B –band luminosity selection, we do not find a significant population of red ($M_{NUV} - M_r \gtrsim 4$), dusty SF ($M_r - M_J \gtrsim 1$) galaxies (i.e., they are faint due to the dust extinction). In contrast, this population appears in NIR-selected samples, as those from Ilbert et al. (2010) or Bundy et al. (2010). To explore in more details the nature of red and blue sources, we use the spectro-photometric types (S_{types}) of the galaxies. These spectro-photometric types were obtained by fitting 62 templates, that include ellipticals and S0’s ($S_{\text{type}} = 1 - 13$), early-type spirals ($S_{\text{type}} = 14 - 29$), late-type spirals ($S_{\text{type}} = 30 - 43$), and irregulars and starburst ($S_{\text{type}} = 44 - 62$; see Zucca et al. 2006, for details). In Fig. 6, we also show the number density contours of $M_B^c \leq -20$ galaxies when we split them into early ($S_{\text{types}} \leq 8$) and late ($S_{\text{types}} > 8$) types. We show that, as expected, red sequence galaxies are mainly ($\sim 90\%$) early types, while blue cloud is populated ($\sim 95\%$) by later types (see also Arnouts et al. 2007). Because of this, and for simplicity, we define red, quiescent galaxies as those with $M_{NUV} - M_r \geq 4.25$, and blue, star-forming galaxies as those with $M_{NUV} - M_r < 4.25$. We note that the trends and main results in this section remain the same if we either vary the blue–red limit by ± 0.25 mag or use spectro-photometric types to define an early (i.e., red) and a late (i.e., blue) population.

With the previous definitions, the principal sample comprises 268 red and 743 blue sources. We look for $r_p^{\max} = 100h^{-1}$ kpc close companions, regardless of their colour, to ensure good statistics. As was mentioned in the previous section, the trends obtained with this search radius are representative to trends observed at smaller separation. We find that:

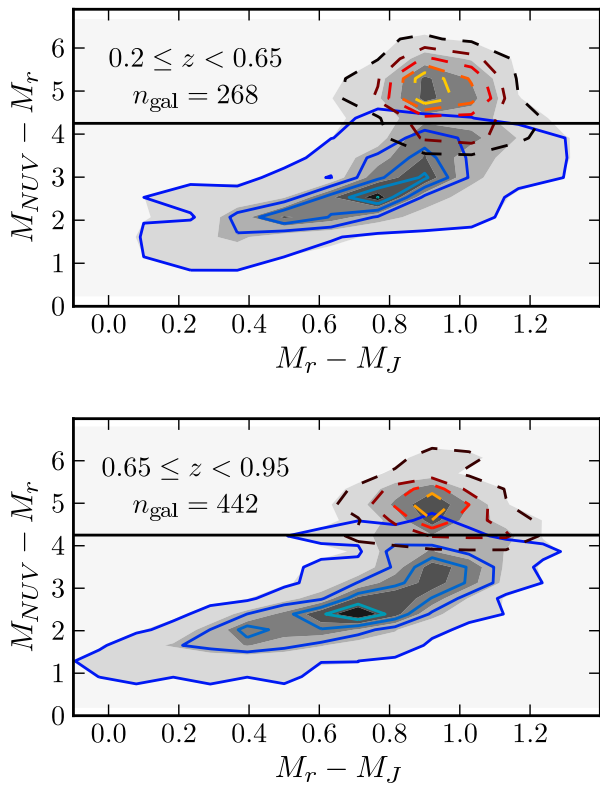


Fig. 6. Number density (gray scales) of $M_B^e \leq -20$ galaxies in the $M_{NUV} - M_r$ versus $M_r - M_J$ plane at $z_{r,1} = [0.2, 0.65]$ (top panel) and $z_{r,2} = [0.65, 0.95]$ (bottom panel). Dashed and solid contours are the number density of early ($S_{type} \leq 8$) and late ($S_{type} > 8$) spectro-photometric types, respectively. We show those galaxies detected in the K band. The number of sources in each interval, n_{gal} , is labeled in the panels. The black solid line is the condition $M_{NUV} - M_r = 4.25$ that we use to split our galaxies into red and blue. [A colour version of this plot is available at the electronic edition].

- The merger fraction of red galaxies (f_m^{red} ; Table 5) is higher than the merger fraction of blue galaxies (f_m^{blue} ; Table 6). For major mergers at $z = 0.8$, both fractions are comparable.
- f_m^{red} evolves little, if any, with cosmic time. Because of this lack of evolution, and to obtain better statistics, we combine both redshift ranges in the following (fourth column in Table 5, and Fig. 7). We find that the power-law index is $s = -0.79 \pm 0.12$ in the range $0.2 \leq z < 0.95$. This implies that red galaxies have a similar number of minor and major companions, $f_{m/M}^{\text{red}} = 1.06 \pm 0.22$.
- f_m^{blue} is lower at $z = 0.5$ than at $z = 0.8$. The observed evolution is faster for higher values of μ (Fig. 7), so we obtain different ($> 2\sigma$) values for the power-law index: $s = -0.52 \pm 0.10$ at $z = 0.8$ and $s = -1.26 \pm 0.20$ at $z = 0.5$. The ratio of minor-to-major companions of blue galaxies grows from $f_{m/M}^{\text{blue}} = 0.61 \pm 0.15$ at $z = 0.8$ to $f_{m/M}^{\text{blue}} = 2.17 \pm 0.57$ at $z = 0.5$.

The fraction of principal galaxies that have a companion and are blue, $f_{\text{blue},1} = N_p^{\text{blue}}/N_p$, does not depend on μ at $z = 0.8$, $f_{\text{blue},1} \sim 70\%$. On the other hand, $f_{\text{blue},1}$ increases when μ decreases at $z = 0.5$, varying from $f_{\text{blue},1} \sim 50\%$ at $\mu \geq 1/10$ to $f_{\text{blue},1} \sim 40\%$ at $\mu \geq 1/4$, in contrast with $\sim 70\%$ at $z = 0.8$. The

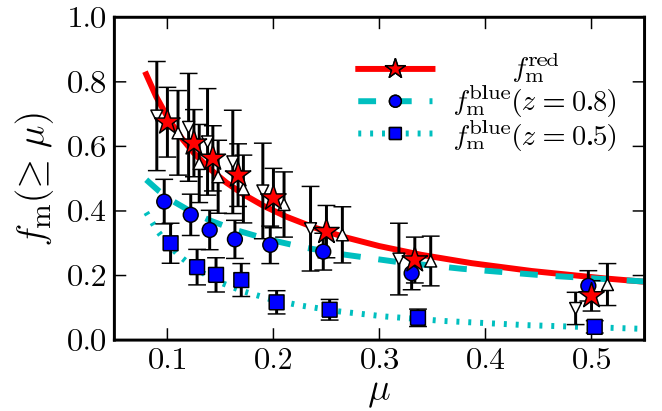


Fig. 7. Merger fraction versus luminosity ratio in B -band, μ . Stars, triangles and inverted triangles are the merger fraction of red primaries, f_m^{red} , at $z \in [0.2, 0.95]$, $z = 0.8$, and $z = 0.5$, respectively. Dots and squares are the merger fraction of blue primaries, f_m^{blue} , at $z = 0.8$ and $z = 0.5$, respectively. The points are shifted when necessary to avoid overlap. The lines are the GLS fits of a power-law function, $f_m(\geq \mu) \propto \mu^s$, to the combined f_m^{red} ($s = -0.79$; solid), f_m^{blue} at $z = 0.8$ ($s = -0.52$; dashed), and f_m^{blue} at $z = 0.5$ data ($s = -1.26$; dotted). [A colour version of this plot is available at the electronic edition].

Table 5. Merger fraction of $L_{B,1} \gtrsim L_B^*$, red ($M_{NUV} - M_r \geq 4.25$) galaxies as a function of luminosity ratio μ for $r_p^{\text{max}} = 100h^{-1}$ kpc

μ	$z = 0.5$	$z = 0.8$	N_p^{red}	$z \in (0.2, 0.95]$
1/2	0.098 ± 0.050	0.174 ± 0.065	8	0.137 ± 0.047
1/3	0.251 ± 0.111	0.246 ± 0.077	14	0.248 ± 0.071
1/4	0.345 ± 0.131	0.324 ± 0.087	19	0.336 ± 0.081
1/5	0.462 ± 0.148	0.418 ± 0.101	25	0.440 ± 0.092
1/6	0.552 ± 0.160	0.467 ± 0.106	29	0.511 ± 0.097
1/7	0.614 ± 0.165	0.523 ± 0.113	32	0.563 ± 0.101
1/8	0.659 ± 0.167	0.562 ± 0.121	35	0.610 ± 0.104
1/10	0.694 ± 0.169	0.655 ± 0.131	39	0.675 ± 0.108

fraction of principal galaxies that have a companion and are red is $f_{\text{red},1} = N_p^{\text{red}}/N_p = 1 - f_{\text{blue},1}$.

We find that the fraction of companions that are blue is $f_{\text{blue},2} \sim 0.8$, regardless either of the colour of the principal or μ . This means that red–red (dry), red–blue or blue–red (mixed), and blue–blue (wet) pairs account for $\sim 10\%/40\%/50\%$ of the pairs with a minor companion in all the redshift range under study. This lack of evolution contrasts with the strong evolution of major mergers, for which the relative fractions are $\sim 5\%/40\%/55\%$ at $z = 0.8$ (similar to the minor ones), and $\sim 10\%/60\%/30\%$ at $z = 0.5$. From $z \sim 0.8$ to $z \sim 0.5$, the fraction of wet major mergers decreases by a factor of two, while dry and mixed mergers increase their importance. Our major merger trends are in agreement with de Ravel et al. (2009) using an expanded data set, as well as previous works, e.g., Lin et al. (2008); Bundy et al. (2009). These results show that the relative fraction of dry and mixed major mergers become more important with cosmic time for $L_B \gtrsim L_B^*$ galaxies in our redshift range due to the lack of blue primaries with major companions at low redshift, rather than

Table 6. Merger fraction of $L_{B,1} \gtrsim L_B^*$, blue ($M_{NUV} - M_r < 4.25$) galaxies as a function of luminosity ratio μ for $r_p^{\max} = 100h^{-1}$ kpc

μ	$z = 0.5$		$z = 0.8$	
	N_p^{blue}	f_m^{blue}	N_p^{blue}	f_m^{blue}
1/2	4	0.041 ± 0.019	16	0.168 ± 0.047
1/3	6	0.069 ± 0.027	20	0.207 ± 0.051
1/4	8	0.094 ± 0.032	27	0.274 ± 0.057
1/5	10	0.117 ± 0.036	30	0.295 ± 0.058
1/6	14	0.186 ± 0.051	32	0.312 ± 0.059
1/7	15	0.202 ± 0.053	35	0.341 ± 0.061
1/8	17	0.226 ± 0.055	39	0.388 ± 0.064
1/10	23	0.300 ± 0.062	41	0.429 ± 0.069

from an increase in the major merger fractions of red galaxies as also pointed out by Lin et al. (2008).

Previous work finds that the major merger fraction from close pairs depends on mass, with more massive galaxies having higher merger fractions (de Ravel et al. 2009; Bundy et al. 2009). If blue principal galaxies at $z = 0.8$ were more massive by a factor of 3 than at $z = 0.5$ because of our B -band luminosity selection, this would explain the observed trend in f_m^{blue} . Using stellar masses determined in Pozzetti et al. (2007), we do not find a significant change (less than 0.1 dex) in the median mass of red, $\log(M_{\star, \text{red}}/M_{\odot}) \sim 10.8$, and blue, $\log(M_{\star, \text{blue}}/M_{\odot}) \sim 10.3$, principal galaxies. This supports that the observed trends reflect a real evolution in the merger properties of blue galaxies. In addition, our results imply that more massive (red) galaxies have higher merger fractions than lower mass (blue) galaxies, in agreement with de Ravel et al. (2009) and Bundy et al. (2009). The study of the major and minor merger fraction in mass selected galaxies is beyond the scope of the present paper, and we will address this issue in a future work.

6. The minor merger rate of $L_B \gtrsim L_B^*$ galaxies

6.1. The minor merger rate of the full population

Our goal in this section is to estimate the minor merger ($1/10 \leq \mu < 1/4$) rate of bright galaxies in the range $0.2 \leq z < 0.95$. In the following we name the *merger rate* the number of mergers per Gyr per galaxy, noted R . Because the parameters involved in the translation of the merger fraction to the merger rate are better constrained for major mergers, we estimate them first and then expand to the minor merger rate.

Following de Ravel et al. (2009), we define the major merger rate as

$$R_{\text{MM}} = f_{\text{MM}} C_p C_m T_{\text{MM}}^{-1}, \quad (9)$$

where the factor C_p takes into account the lost companions in the inner $5h^{-1}$ kpc (Bell et al. 2006) and the factor C_m is the fraction of the observed close pairs that finally merge in a typical timescale T_{MM} . We take $C_p = r_p^{\max}/(r_p^{\max} - 5h^{-1} \text{ kpc})$. The typical merger timescale depends on r_p^{\max} and can be estimated by cosmological and N -body simulations. We compute the major merger timescales from the cosmological simulations of Kitzbichler & White (2008), based on the Millennium simulation (Springel et al. 2005). These major merger timescales, denoted T_{MM}^{K08} , refer to major mergers ($\mu > 1/4$ in stellar mass), and

depend mainly on r_p^{\max} and on the stellar mass of the principal galaxy, with a weak dependence on redshift in our range of interest (see de Ravel et al. 2009, for details). Taking $\log(M_{\star}/M_{\odot}) = 10.7$ as the average stellar mass of our principal galaxies with a close companion, we obtain the values in Table 7 for $r_p^{\max} = 30$, 50 and $100 h^{-1}$ kpc, and $\Delta v^{\max} = 500 \text{ km s}^{-1}$. In every case we assume an uncertainty of 0.2 dex in the mass of the principal galaxies to estimate the error in T_{MM}^{K08} . These timescales already include the factor C_m (see Patton & Atfield 2008; Bundy et al. 2009; Lin et al. 2010), so we take $C_m = 1$ in the following. These timescales are for central - satellite mergers, and satellite - satellite pairs could have different timescales. However, only 1 of the 103 close pairs under study is satellite - satellite, so the use of principal - satellite timescales is justified. We also remark that the velocity condition $\Delta v^{\max} = 500 \text{ km s}^{-1}$ selects close bound systems even when they are located in dense environments, but in these environments the probability of finding unbound close pairs increases. This is taken into account in the cosmological averaged merger timescales (see also Lin et al. 2010).

Since the assumed merger timescale is the most uncertain quantity in Eq. (9), we compare T_{MM}^{K08} with other recent estimations in the literature. Lotz et al. (2010b) perform N -body/hydrodynamical simulations of major and minor mergers to study the merger timescales of morphological and close pair approaches. The principal galaxy in their simulations has $\log(M_{\star}/M_{\odot}) = 10.7$, similar to the average mass of our principal galaxies with a close companion, so their major merger timescales, denoted T_{MM}^{JL10} , should be comparable to the previous T_{MM}^{K08} . We summarize the average values of T_{MM}^{JL10} in Table 7 after correcting with the factor C_p . We find that $T_{\text{MM}}^{JL10} < T_{\text{MM}}^{K08}$. However, the T_{MM}^{K08} include the factor C_m , while the T_{MM}^{JL10} do not. Applying to T_{MM}^{JL10} a typical value of $C_m = 0.6$ (Patton et al. 2000; Lin et al. 2004, 2010; Bell et al. 2006), we find that *both timescales agree and therefore yield similar merger rates*. On the other hand, Lin et al. (2010) use cosmological simulations to study C_m and the merger timescale, denoted T_{MM}^{LL10} . They find $T_{\text{MM}}^{LL10} \sim 1.4 \text{ Gyr}$ for $\log(M_{\star}/M_{\odot}) \sim 10.3$ galaxies and $r_p \leq 50h^{-1}$ kpc (this value includes the factor $C_m = 0.7$ derived from their simulations). This timescale is lower by a factor of two than the one from Kitzbichler & White (2008) for this mass, $T_{\text{MM}}^{K08} = 2.7 \text{ Gyr}$. However, Kitzbichler & White (2008) assume that the galaxy merger occurs a dynamical friction time after the dark matter halo merger; while Lin et al. (2010) do not consider this extra time. This fact mitigates the difference between both works, but a more detailed comparison is needed. In the following we omit the super index in T_{MM}^{K08} for clarity.

The merger rate is an absolute quantity, and should not depend on the r_p^{\max} that we use to infer it. Because of this, the increase of the merger fraction with r_p^{\max} (Sect. 4, Fig. 4) must be compensated with the increase in T_{MM} . For two different search radius, $r_{p,1}^{\max}$ and $r_{p,2}^{\max}$, this implies that

$$\Delta T_{\text{MM}}(r_{p,1}^{\max}, r_{p,2}^{\max}) = \frac{T_{\text{MM}}(r_{p,1}^{\max})}{T_{\text{MM}}(r_{p,2}^{\max})} = \frac{C_{p,1}}{C_{p,2}} \left(\frac{r_{p,1}^{\max}}{r_{p,2}^{\max}} \right)^q. \quad (10)$$

From our observational results we infer that $\Delta T_{\text{MM}}(50, 30) = 1.5$ and $\Delta T_{\text{MM}}(100, 50) = 1.8$. These values compare nicely with the ratios from Table 7 timescales, $\Delta T_{\text{MM}}(50, 30) = 1.6$ and $\Delta T_{\text{MM}}(100, 50) = 1.8$. This supports the robustness of the assumed T_{MM} , although the normalization of these timescales have a factor of two uncertainty. We estimate the final major merger rate averaging the values derived from the 30, 50 and $100h^{-1}$

Table 7. Major merger timescales of $L_{B,1} \gtrsim L_B^*$ galaxies

r_p^{\max} (h^{-1} kpc)	T_{MM}^{K08} (Gyr)	T_{MM}^{JL10} (Gyr)	T_{MM}^{JL10}/C_m (Gyr)
30	1.4 ± 0.2	0.9	1.5
50	2.3 ± 0.3	1.5	2.5
100	4.2 ± 0.5	2.4	4.0

kpc merger fractions, and its error as the average of the individual merger rates' errors.

We obtain the minor merger rate, defined as the merger rate of $1/10 \leq \mu < 1/4$ close pairs, from the major one as

$$R_{\text{mm}} = f_{m/M} \frac{R_{\text{MM}}}{\Upsilon}, \quad (11)$$

where the factor Υ accounts for the difference in the minor merger timescale with respect to the major merger one in close pairs, $T_{\text{mm}} = \Upsilon \times T_{\text{MM}}$. Only a few studies in the literature attempt to estimate Υ : Jiang et al. (2008) study the merger timescale of dark matter haloes, finding $\Upsilon \sim 2$. On the other hand, Lotz et al. (2010b) obtain $\Upsilon = 1.5 \pm 0.1$ from N -body/hydrodynamical simulations. As we have already shown, the major merger timescales from Lotz et al. (2010b) are similar to ours, so we assume the minor-to-major merger time scale from Lotz et al. (2010b) in the following. We also assume that the factor C_m for minor mergers is the same as the one for major mergers.

Finally, the total merger rate is $R_m = R_{\text{MM}} + R_{\text{mm}}$. We summarize our results on the merger rates in Table 8, and we show them in the Fig. 8. We find that

1. The minor merger rate R_{mm} ($1/10 \leq \mu < 1/4$) decreases with increasing redshift, although our measurements are consistent with a constant minor merger rate within errors. We further discuss the evolution of R_{mm} in Sect. 7.3. This is the first quantitative measurement of the minor merger rate using close pair statistics at these redshifts.
2. This trend is clearly different from the evolution of the major merger rate ($\mu \geq 1/4$) which we find is increasing with redshift, in agreement with de Ravel et al. (2009), and to previous studies in the literature (e.g., Le Fèvre et al. 2000; Conselice et al. 2003, 2009; López-Sanjuan et al. 2009b; Bridge et al. 2010).
3. The total merger rate (major + minor) is consistent either with a mild increase with redshift or with a constant $R_m \sim 0.1 \text{ Gyr}^{-1}$.

6.2. The minor merger rate of red and blue galaxies

We apply the steps in the previous section to estimate the major, minor and total merger rate of red and blue galaxies. We take $T_{\text{MM}}^{\text{red}} = 3.9 \text{ Gyr}$ and $T_{\text{MM}}^{\text{blue}} = 4.8 \text{ Gyr}$ for $r_p^{\max} = 100h^{-1}$ kpc because of the different average stellar mass of red and blue principal galaxies, while the factor Υ does not depend on the gas content of the galaxies (Lotz et al. 2010a). The merger rates that we obtain are listed in Table 8. The merger rates (minor and major) of red galaxies do not evolve with redshift in the range under study, $R_{\text{mm}}^{\text{red}} = 0.064 \text{ Gyr}^{-1}$ and $R_{\text{MM}}^{\text{red}} = 0.091 \text{ Gyr}^{-1}$. González-García et al. (2009) find that the minor and major merger rate of Elliptical Like Objects (ELOs) at $z \sim 0.75$

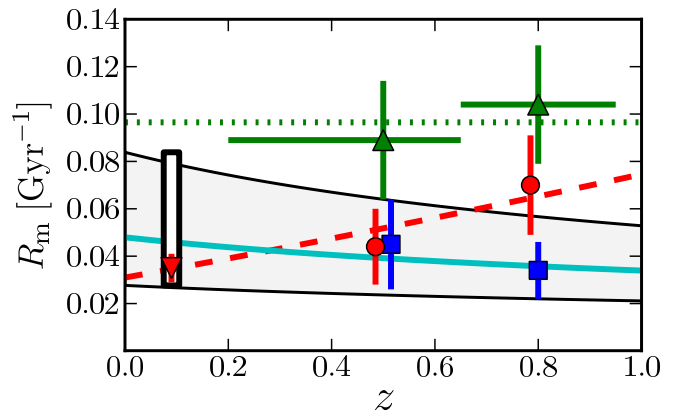


Fig. 8. Merger rate of $M_B^e \leq -20$ galaxies versus redshift. Dots are the major merger rate ($\mu \geq 1/4$), squares are the minor merger rate ($1/10 \leq \mu < 1/4$), and triangles are the total (major + minor, $\mu \geq 1/10$) merger rate. The points are shifted when necessary to avoid overlap. The z error bars in the total merger rate mark the redshift range spanned by VVDS-Deep data. The inverted triangle is the major merger rate of $M_B^e \leq -20$ galaxies from MGC at $z = 0.09$. The white rectangle identifies the local ($z = 0.09$) minor merger fraction estimated from the total and the major merger ones, while the gray area marks the most probable minor merger rate values in the range $0 < z < 1$ (see text for details). The solid line is the best fit of a power-law function with a fixed index, $f_{\text{mm}} \propto (1+z)^{-0.5}$, to the minor merger rate data. The dashed line is the least-squares fit of a power-law function to the major merger rate data. The dotted line is the major + minor merger rate if it is assumed constant. [A colour version of this plot is available at the electronic edition].

in their cosmological simulations are $R_{\text{mm}} = 0.06 \text{ Gyr}^{-1}$ and $R_{\text{MM}} = 0.08 \text{ Gyr}^{-1}$, in good agreement with our observed values. On the other hand, Stewart et al. (2009) model predicts that $R_{\text{mm}} \sim R_{\text{MM}}$ for $\mu_{\text{MM}} = 1/3$ (see also Hopkins et al. 2009c), while from our observations we infer $R_{\text{mm}} = 1.1 \times R_{\text{MM}}$ for $\mu_{\text{MM}} = 1/3$.

The minor merger rate of blue galaxies, denoted $R_{\text{mm}}^{\text{blue}}$, increases by $\sim 20\%$ from $z = 0.8$ to $z = 0.5$, but the measured values are compatible with a constant merger rate within error bars, $R_{\text{mm}}^{\text{blue}} \sim 0.027 \text{ Gyr}^{-1}$. To the contrary, the major merger rate, denoted $R_{\text{MM}}^{\text{blue}}$, decreases by a factor of three from $z = 0.8$ to $z = 0.5$, as noted by de Ravel et al. (2009). These trends suggest that the stability or increase with cosmic time of the minor merger rate found in the previous section is a consequence of the evolution in the fraction of bright galaxies that are red: as time goes by, the red fraction increases (e.g., Fontana et al. 2009; Ilbert et al. 2010). Because the minor merger rate of red galaxies is a factor of ~ 2.5 higher than the one of blue galaxies, and both are roughly constant, the increase in the red fraction implies an increase in the global (red+blue) minor merger rate. This effect is also present in the major merger rate, but in this case $R_{\text{MM}}^{\text{blue}}$ decreases with cosmic time, and the increase in the red fraction is only a mild evolution, as found by de Ravel et al. (2009).

6.3. The volumetric minor merger rate

The volumetric merger rate (i.e., the number of mergers per unit volume and time) is a complementary measure to the merger rate estimated in the previous sections. To obtain the volumetric merger rate, denoted \mathfrak{R} , we multiply the merger rate by

Table 8. Minor, major and total merger rate of $L_B \gtrsim L_B^*$ galaxies

Merger rate (Gyr $^{-1}$)	All galaxies		$z \in [0.2, 0.95]$	Red galaxies		Blue galaxies	
	$z = 0.50$	$z = 0.80$		$z = 0.50$	$z = 0.80$	$z = 0.50$	$z = 0.80$
R_{MM}	0.044 ± 0.016	0.070 ± 0.021	0.091 ± 0.025	0.021 ± 0.007	0.060 ± 0.014		
R_{mm}	0.045 ± 0.019	0.034 ± 0.012	0.064 ± 0.022	0.030 ± 0.013	0.024 ± 0.008		
R_{m}	0.089 ± 0.025	0.104 ± 0.025	0.155 ± 0.033	0.051 ± 0.015	0.084 ± 0.016		

the number density of all/red/blue galaxies with $M_B^e \leq -20$ in VVDS-Deep at each redshift (Ilbert et al. 2005). We summarize the values of \mathfrak{R} in Table 9. All trends are similar to those found in the previous section. Interestingly, we find that $\mathfrak{R}_{\text{mm}}^{\text{red}} \sim \mathfrak{R}_{\text{mm}}^{\text{blue}} \sim 3.5 \times 10^{-5} \text{ Mpc}^{-3} \text{ Gyr}^{-1}$. The merger rate of red galaxies is higher by a factor of ~ 2.5 than that of the blue ones, but the number density of the latter is higher than of the former, hence making the volumetric merger rates comparable.

7. Discussion

In this section we estimate the evolution of the minor merger fraction and rate with redshift, and discuss the contribution of minor mergers to the evolution of bright galaxies since $z \sim 1$, comparing it to the contribution of major mergers.

7.1. The evolution of the minor merger fraction with redshift

The evolution of the merger fraction with redshift up to $z \sim 1.5$ is well parametrized by a power-law (e.g., Le Fèvre et al. 2000; López-Sanjuan et al. 2009b; de Ravel et al. 2009),

$$f_{\text{m}}(z) = f_{\text{m},0} (1+z)^m. \quad (12)$$

Our results alone suggest that the merger fraction evolves faster for higher μ , with $m = 5.6$ for equal luminosity companions ($\mu = 1$), $m = 2.4$ for major companions with $\mu \geq 1/4$, and $m = 0.8$ for major + minor companions ($\mu \geq 1/10$). This mild evolution in the total (major + minor) merger fraction is also suggested by the morphological studies of Lotz et al. (2008) and Jogege et al. (2009).

To better constrain the evolution with redshift of the minor merger fraction, a local reference is important. Darg et al. (2010) estimate that the minor merger fraction is similar to the major one ($f_{\text{m}/M} \sim 1$, $\mu \gtrsim 1/3$) in Galaxy Zoo³ (Lintott et al. 2008); the latter is based on the visual classification of Sloan Digital Sky Survey (SDSS⁴, Adelman-McCarthy et al. 2006) galaxies by internet users. However, their sample is incomplete for minor companions, so their $f_{\text{m}/M}$ is a lower limit. On the other hand, Woods & Geller (2007) study the different properties of major ($\Delta m_z < 2$, $\mu \gtrsim 1/7$) and minor ($\Delta m_z > 2$, $\mu \lesssim 1/7$) close pairs in SDSS. Unfortunately, they do not attempt to derive merger fractions, but the influence of close companions on galaxy properties (see also Ellison et al. 2008; Patton et al. 2011). Therefore, to our knowledge, there does not seem to be any local estimation of the minor merger fraction of bright galaxies in the literature. As a close proxy, we estimate the local merger fraction as $f_{\text{mm}} = f_{\text{m}}(\mu \geq 1/10) - f_{\text{MM}}$. We follow the methodology in Sect. 3 to measure the major ($\mu \geq 1/4$) merger fraction of $M_B^e \leq$

-20 galaxies at $z = 0.09$ from the Millennium Galaxy Catalogue (MGC⁵, Liske et al. 2003). This survey comprises 10095 galaxies with $B_{\text{MGC}} < 20$ over 37.5 deg^2 , with a spectroscopic completeness of 96% (Driver et al. 2005; see also De Propris et al. 2005, 2007). We obtain $f_{\text{MM}}^{\text{MGC}} = 0.139 \pm 0.009$ for $r_p^{\text{max}} = 100h^{-1}$ kpc. We then assume two different types of evolution for the major + minor merger fraction: (1) a constant evolution with redshift, $f_{\text{m}}(\mu \geq 1/10) = 0.461$ for $r_p^{\text{max}} = 100h^{-1}$ kpc, which implies $f_{\text{mm}}(0.09) = 0.322$; and (2) an evolution which evolves with redshift as $m = 0.8$ (fit of a power-law function to our observational major + minor merger fractions), which implies $f_{\text{mm}}(0.09) = 0.187$. Finally, we fit Eq. (12) to our minor merger fraction data and both local estimates, defining a confidence area for the minor merger fraction between $z = 0$ and $z = 1$ (Fig. 5). This area is limited by the following curves,

$$f_{\text{mm}}^{\text{up}} = 0.393 (1+z)^{-0.32}, \quad (13)$$

$$f_{\text{mm}}^{\text{down}} = 0.182 (1+z)^{-0.25}. \quad (14)$$

The power law-index from the fits is $m = -0.4 \pm 0.7$. The negative value implies that the minor merger fraction decreases with increasing redshift. We note that our results are compatible with a constant f_{mm} since $z = 1$ (i.e., $m = 0$). Even in that case, the minor merger fraction does not evolve in the same way as the major one, that increases with redshift ($m > 0$, see below). Abbas et al. (2010) use Halo Occupation Distribution (HOD) models to interpret the evolution since $z \sim 1$ of the correlation function from VVDS-Deep (see also Le Fèvre et al. 2005a) and SDSS. Their results suggest that the average number of satellite galaxies per dark matter halo increases with cosmic time, which could be related with our suggested increase in the minor merger fraction. Specifically, we expect the minor merger fraction in the local universe to be two to three times the major merger one. Direct measurements of the minor merger fraction at low redshift will be needed to better constrain the minor merger fraction evolution with z .

The least-squares fit to the major merger data yields (Fig. 5)

$$f_{\text{MM}} = (0.116 \pm 0.024) (1+z)^{1.3 \pm 0.5}. \quad (15)$$

In a previous work in VVDS-Deep, de Ravel et al. (2009) measured the major merger fraction ($\mu \geq 1/4$) of less luminous galaxies than those reported in present paper. They find that the major merger fraction evolves faster with z for fainter samples, with a power-law index $m = 4.7$ for $M_B^e \leq -18$ galaxies and $m = 3.1$ for $M_B^e \leq -18.77$ galaxies. The evolution of $m = 1.3$ for the major merger fraction of $M_B^e \leq -20$ galaxies confirms the trend found by de Ravel et al. (2009) and extends it to brighter galaxies.

³ <http://www.galaxyzoo.org>

⁴ <http://sdss.org/>

⁵ <http://eso.org/~jliske/mgc/>

Table 9. Minor, major and total volumetric merger rate of $L_B \gtrsim L_B^*$ galaxies

Merger rate ($\times 10^{-5}$ Mpc $^{-3}$ Gyr $^{-1}$)	All galaxies		$z \in [0.2, 0.95]$	Red galaxies		Blue galaxies	
	$z = 0.50$	$z = 0.80$		$z = 0.50$	$z = 0.80$	$z = 0.50$	$z = 0.80$
\mathfrak{R}_{MM}	8.3 ± 3.0	12.6 ± 3.8		4.4 ± 1.2	2.8 ± 1.0	8.3 ± 1.9	
\mathfrak{R}_{mm}	8.6 ± 3.6	6.1 ± 2.2		3.1 ± 1.1	4.0 ± 1.8	3.4 ± 1.2	
\mathfrak{R}_m	16.8 ± 4.7	18.8 ± 4.4		7.5 ± 1.6	6.8 ± 2.0	11.7 ± 2.3	

7.2. The evolution of the power-law index s with redshift

In a previous study, López-Sanjuan et al. (2010a) have attempted to measure the power-law index s . They find $s \sim -0.6$ at $z \in [0.2, 1.1]$ for principal galaxies with $M_\star \gtrsim 10^{10} M_\odot$. This value is similar to ours at $z = 0.8$, but at $z \sim 0.5$ the discrepancy between both studies is important ($> 2\sigma$). This suggests that s depends not only on both redshift and colour, but also on stellar mass. Because the B -band luminosities of red galaxies are only slightly affected by star formation, our red merger fraction is a proxy of the merger fraction of $\log(M_\star/M_\odot) \sim 10.8$ galaxies. We therefore find that the power-law index does not evolve for massive galaxies, $s = -0.79 \pm 0.12$. This, combining with López-Sanjuan et al. (2010a) results, suggests that (i) s does not evolve with z in mass-selected samples; that is, the evolution of the total (major + minor) merger fraction is similar to that of the major merger one, as predicted by the cosmological models of Stewart et al. (2009), and (ii) the power-law index is lower for massive galaxies indicating that massive galaxies have a higher minor-to-major merger ratio than less massive ones. The minor merger fraction in different mass-selected samples will be the subject of a future work to expand on results presented here.

7.3. The redshift evolution of the minor merger rate

Similarly to the minor merger fraction, there does not seem to exist any published reference in the refereed literature for the local minor merger rate. We follow the same steps as in Sect. 7.1 to estimate a confidence area for the minor merger rate in the range $0 < z < 1$. The major merger rate in the MCG at $z = 0.09$ is $R_{\text{MM}}^{\text{MCG}} = 0.035 \pm 0.006$ Gyr $^{-1}$, while the confidence area is limited by the following curves (Fig. 8),

$$R_{\text{mm}}^{\text{up}} = 0.084(1+z)^{-0.67}, \quad (16)$$

$$R_{\text{mm}}^{\text{down}} = 0.028(1+z)^{-0.39}. \quad (17)$$

The power law-index inferred from the fits is $n = -0.5 \pm 0.7$. As in Sect. 7.1, a negative power-law index for R_{mm} implies that the minor merger rate decreases with redshift. Also in this case the value of n is compatible with a constant minor merger rate ($n = 0$), but again its evolution is different than that of the major merger rate, that increases with redshift ($n > 0$, see below). A local reference is needed to better constraint the evolution of R_{mm} . If we repeat this study with the volumetric merger rate, the confidence area is limited by

$$\mathfrak{R}_{\text{mm}}^{\text{up}} = 11.3(1+z)^{0.19} \times 10^{-5} \text{ Mpc}^{-3} \text{ Gyr}^{-1}, \quad (18)$$

$$\mathfrak{R}_{\text{mm}}^{\text{down}} = 6.8(1+z)^{-0.91} \times 10^{-5} \text{ Mpc}^{-3} \text{ Gyr}^{-1}. \quad (19)$$

In this case the evolution is $n = -0.5 \pm 0.7$.

The fit to both major merger rates is

$$R_{\text{MM}} = (0.031 \pm 0.006)(1+z)^{1.3 \pm 0.6}, \quad (20)$$

$$\mathfrak{R}_{\text{MM}} = (6.6 \pm 1.2)(1+z)^{0.9 \pm 0.4} \times 10^{-5} \text{ Mpc}^{-3} \text{ Gyr}^{-1}. \quad (21)$$

de Ravel et al. (2009) estimate the volumetric major merger rate ($\mu \geq 1/4$) finding, as for the merger fraction, that it evolves faster for fainter samples, with a power-law index $n = 2.2$ for $M_B^e \leq -18$ galaxies and $n = 1.6$ for $M_B^e \leq -18.77$ galaxies, so our $n = 0.9$ follows the trend of decreasing n for brighter galaxies found by de Ravel et al. (2009). On the other hand, the volumetric merger rate of $M_B^e \leq -18$ galaxies is a factor of ~ 5 higher than the one of $M_B^e \leq -20$ galaxies. This is because the number density is lower for bright galaxies than for the fainter ones. The same trend is observed in mass-selected samples (López-Sanjuan et al. 2009a).

7.4. The role of minor mergers in the mass assembly of luminous galaxies

We can obtain the average number of mergers per galaxy between z_2 and $z_1 < z_2$ as

$$N_m = \int_{z_1}^{z_2} R_m \frac{dz}{(1+z)H_0 E(z)}, \quad (22)$$

where $E(z) = \sqrt{\Omega_\Lambda + \Omega_m(1+z)^3}$ in a flat universe. The definitions of N_{MM} and N_{mm} are analogous. Using results from the previous section, we obtain $N_m = 0.73 \pm 0.21$, with $N_{\text{MM}} = 0.37 \pm 0.13$ and $N_{\text{mm}} = 0.36 \pm 0.17$ from $z = 1$ to $z = 0$, indicating that *the number of minor mergers per bright galaxy since $z = 1$ is similar to the number of major ones*. Note that these values and those reported in the following have an additional factor of two uncertainty due to the merger timescales derived from simulations (Sect. 6.1). In their work, Pozzetti et al. (2010) find that almost all the evolution in the stellar mass function since $z \sim 1$ is consequence of the observed star formation (see also Vergani et al. 2008), and estimate $N_m \sim 0.7$ mergers since $z \sim 1$ per $\log(M_\star/M_\odot) \sim 10.6$ galaxy, similar to the average mass of our $M_B^e \leq -20$ galaxies, are needed to explain the remaining evolution. Their result agrees with our direct estimation, but they infer $N_{\text{MM}} < 0.2$. This value is half of ours, pointing out that close pair studies are needed to understand accurately the role of major/minor mergers in galaxy evolution.

In addition to the mean number of mergers per galaxy, we have estimated the mass accreted by bright galaxies since $z = 1$ due to major and minor mergers. For this, we take μ as a proxy of the mass ratio between the galaxies in the pair. We can determine the mean merger ratio of major ($\overline{\mu_{\text{MM}}}$), and minor mergers ($\overline{\mu_{\text{mm}}}$) as

$$\overline{\mu_{\text{MM}}} = \frac{s}{s+1} \frac{1 - \mu_{\text{MM}}^{s+1}}{1 - \mu_{\text{MM}}^s}, \quad (23)$$

$$\overline{\mu_{\text{mm}}} = \frac{s}{s+1} \frac{\mu_{\text{mm}}^{s+1} - \mu_{\text{MM}}^{s+1}}{\mu_{\text{mm}}^s - \mu_{\text{MM}}^s}. \quad (24)$$

For $\mu_{\text{MM}} = 1/4$ and $\mu_{\text{mm}} = 1/10$ we obtain $\overline{\mu_{\text{MM}}} = 0.47$ and $\overline{\mu_{\text{mm}}} = 0.15$, values that depend slightly on s : the mean merger

ratios change less than 10% in the range probed by our results, $s \in [-1.25, -0.58]$. We assume these values of $\overline{\mu_{\text{MM}}}$ and $\overline{\mu_{\text{mm}}}$ hereafter. Weighting the number of mergers with its corresponding merger ratio, we infer that *mergers of companions with μ in the range 1/10 to 1 increase the mass of bright galaxies since $z = 1$ by $23 \pm 8\%$* . We further infer that the relative contribution of major and minor mergers to this mass assembly is 75% and 25%, respectively. Because the factor of two uncertainty in the merger timescales affects in the same way major and minor mergers, this relative contribution is a robust result. In their cosmological models, Hopkins et al. (2010a) predict that the relative contribution of major and minor mergers in the spheroids assembly of $\log(M_\star/M_\odot) \sim 10.6$ galaxies is $\sim 80\%/20\%$, in good agreement with our observational result.

Therefore, we have demonstrated that minor mergers do contribute to the mass assembly of bright galaxies, at a level corresponding to about a third of the major mergers contribution.

7.5. Mergers and the evolution of red galaxies since $z \sim 1$

Because the merger properties of red and blue galaxies are very different, we estimate here the role of minor and major mergers in the evolution of red galaxies since $z \sim 1$. We assume a constant major and minor merger rate for red galaxies from $z = 0$ to $z = 1$, as found in Section 6. Applying Eq. (22) to $R_{\text{mm}}^{\text{red}}$ and $R_{\text{MM}}^{\text{red}}$, we obtain that *the average number of mergers per red galaxy since $z = 1$ is $N_m^{\text{red}} = 1.2 \pm 0.3$, with $N_{\text{MM}}^{\text{red}} = 0.7 \pm 0.2$ and $N_{\text{mm}}^{\text{red}} = 0.5 \pm 0.2$* . These values are higher than those from the global population, reflecting the higher merger rate of red galaxies.

We find that red galaxies of $\log(M_\star/M_\odot) \sim 10.8$ have undergone ~ 1.2 merger events since $z \sim 1$, but it is important to quantify the impact of mergers in the mass assembly of these galaxies. Weighting the number of mergers with their corresponding mean merger ratio (Eqs. [23] and [24]), we find that *mergers can increase 40 \pm 10% the mass of red galaxies since $z = 1$* . Because blue companions have a lower mass-to-light ratio than the red ones, this mass increase is an upper limit. The relative contribution of major/minor mergers to this mass assembly is 80%/20%, indicating that the mass of red galaxies increases by $\sim 10\%$ since $z = 1$ due to minor mergers.

Several authors have studied the luminosity function (LF) and the clustering to constrain the evolution of luminous red galaxies (LRGs) with redshift. They find that the bright end ($L \gtrsim 2.5L^*$) of the LF is mostly in place since $z \sim 0.8$ (e.g., Zucca et al. 2006; Brown et al. 2007; Scarlata et al. 2007). Since LRGs have a negligible star formation (Roseboom et al. 2006), the evolution of the bright end of the LF, if any, must be due to mergers. Brown et al. (2008) find that bright LRGs ($M_B \lesssim -21.8 \sim 4L^*$) have increased their mass $\sim 30\%$ since $z = 1$ (see also Brown et al. 2007), in agreement with our result. Cool et al. (2008) state that $L > 3L^*$ galaxies have increased their stellar mass less than 50% since $z \sim 0.9$, an upper limit also consistent with our measurement. On the other hand, van Dokkum et al. (2010) study the evolution of massive galaxies with $\log(M_\star/M_\odot) \gtrsim 11.3$ since $z \sim 2$, inferring that they increase their mass $\sim 40\%$ since $z \sim 1$ to the present by mergers (i.e., their star-formation is negligible in that redshift range, see also Walcher et al. 2008 and Drory & Alvarez 2008), in good agreement with our direct measurement. Although the stellar mass and luminosity range probed by van Dokkum et al. (2010) and previous LF works is ~ 3 times higher than ours, and we use B -band luminosity as a proxy of mass, the agreement

with these studies is remarkable and supports that mergers are an important contributor to the evolution of the most massive red galaxies since $z \sim 1$.

While mergers directly increase the mass in red galaxies, they also modify their inner structure. It is now well established that massive, $\log(M_\star/M_\odot) \gtrsim 11$, early-type galaxies have, on average, lower effective radius (r_e) at high redshift than locally, being ~ 2 to ~ 4 times smaller at $z \sim 1$ and $z \sim 2$, respectively (Daddi et al. 2005; Trujillo et al. 2006, 2007; Buitrago et al. 2008; van Dokkum et al. 2008, 2010; van der Wel et al. 2008; Toft et al. 2009; Williams et al. 2010). These high-redshift compact galaxies are sparse in the local universe (Trujillo et al. 2009; Taylor et al. 2010), implying that they evolve since $z \sim 2$ to the present. It has been suggested that compact galaxies are the cores of present day ellipticals, and that they increase their size by adding stellar mass in the outskirts of the galaxy (Bezanson et al. 2009; Hopkins et al. 2009a; van Dokkum et al. 2010). Equal-mass mergers ($\mu = 1$) are efficiently increasing the mass of the galaxies, but not their size ($r_e \propto M_\star$); while for un-equal mass mergers ($\mu < 1$) the size increase is higher for the same accreted mass ($r_e \propto M_\star^2$; Bezanson et al. 2009; Hopkins et al. 2010b). We find that red galaxies increase their mass $\sim 40\%$ since $z \sim 1$ due primarily to un-equal mass mergers. This corresponds to a size increase by a factor of ~ 2 , which is similar to the growth derived by size studies. Our results therefore suggest that un-equal mass mergers ($\mu < 1$) could be the dominant process in the size growth of massive galaxies since $z \sim 1$, as predicted by the cosmological simulations of Naab et al. (2009) or Hopkins et al. (2010b). Future studies of the merger fraction as a function of the size of galaxies are needed to better understand the evolution of compact galaxies.

Kaviraj et al. (2011) found that $\sim 30\%$ of early types at $0.5 < z < 0.7$ present distorted morphologies. This fraction is $\sim 25\%$ if we restrict the analysis to $M_V \lesssim -21.5$ galaxies (this selects $M_B^e \lesssim -20$ galaxies at $z = 0.6$ assuming $B - V = 0.7$, the main $M_B - M_V$ colour of our red galaxies in the range $0.5 < z < 0.7$). Interestingly, Conselice et al. (2007) also found that $\sim 25\%$ of the early-types with $\log(M_\star/M_\odot) \geq 10.8$ in the Palomar/DEEP2 survey present signs of interactions at these redshifts. If we assume a visibility timescale of $T_{\text{dET}} \sim 1$ Gyr for Kaviraj et al. (2011) distorted early-types (dET), we need a total (major + minor) merger rate of $R_{\text{dET}} \sim 0.25$ Gyr $^{-1}$ to explain the observed fraction of dET. This value is higher than our red merger rate, $R_m^{\text{red}} = 0.155 \pm 0.033$ Gyr $^{-1}$, but we infer an additional $R_{\text{dET}}^{\text{blue}} \sim 0.1$ from the major merger rate of blue galaxies, that can also lead to dET (Sect. 7.6). Mergers could therefore be common enough to explain the observed frequency of dET at $z = 0.6$, with minor mergers accounting for $\sim 30\%$ of the observed dET. N -body simulations are needed to better determine T_{dET} and the minimum μ that produces observable tidal features. We also note that minor mergers with luminosity or mass ratios less than 1/10 may also contribute significantly, and will need to be investigated.

Kaviraj et al. (2011) also show that the majority of dET have blue $NUV - r$ rest-frame colours, a signature of episodes of recent star formation (RSF). The fraction of the stellar mass formed in the RSF is $f_{\star, \text{RSF}} \sim 3\%-20\%$ (see also Scarlata et al. 2007; Kaviraj et al. 2008), while the derived metallicity makes unlikely gas-rich mergers as the origin of this RSF. We find that $\sim 80\%$ of the companions of the red primaries are blue indicating that there is a gas supply to the RSF, while the stellar mass is dominated by the red, old component of both galaxies. Using the recipe provided by Stewart et al. (2009) to determine M_{gas}/M_\star , where M_{gas} is the mass of gas in the galaxy, we explore the mass

and μ range of our red pairs, and estimate that the gaseous mass is typically $\lesssim 25\%$ of the total stellar mass in our red pairs. Simulations suggest that $\sim 50 - 75\%$ of the gas in mergers can be consumed to form new stars (Cox et al. 2004, 2006). This leads to a $f_{\star,RSF} \lesssim 20\%$, in agreement with the observed mass formed in the RSF episodes. This result is supporting mergers as the main cause of RSF in early-type galaxies since $z \sim 1$ (see also Fernández-Ontiveros et al. 2011).

Bundy et al. (2010) find that the red sequence is populated not only by E/S0 galaxies, but also by passive, early-type (i.e., bulge dominated) spirals. While 80% of the mergers experienced by a red galaxy are with a blue SF companion, the low gaseous mass involved in these mergers ($\lesssim 25\%$) prevent the regrowth of a spiral disc (Hopkins et al. 2009b). Hence, our observed merger rate could be enough to transform the red, early-type spirals into E/S0 galaxies. A more detailed study of the merger fraction of red galaxies as a function of their morphology is needed to understand the transition between red spirals and E/S0 galaxies.

Summarizing, our measured merger rates of bright red galaxies are in agreement with the mass and size evolution of massive red galaxies since $z = 1$, and with the frequency of distorted early-type galaxies at $z \sim 0.6$. Minor mergers have a significant impact in the evolution of these massive red galaxies, accounting of $\sim 20\%$ of the observed evolution.

7.6. The role of minor mergers in the evolution of blue galaxies

Observations and N -body simulations suggest that major mergers between gas-rich late-type galaxies are an efficient way to obtain quiescent, early-type galaxies (Naab et al. 2006; Rothberg & Joseph 2006a,b; Rothberg & Fischer 2010; Hopkins et al. 2008, 2009b). Recent studies find that gas-rich major mergers can only account for 20%-30% of the number density evolution in the red sequence of intermediate-mass ($M_{\star} \gtrsim 10^{10} M_{\odot}$) galaxies since $z = 1$ (Bundy et al. 2009; Wild et al. 2009; de Ravel et al. 2009; López-Sanjuan et al. 2010b,a), while major mergers are enough to explain the number evolution of massive galaxies in the same redshift range ($M_{\star} \gtrsim 10^{11} M_{\odot}$, Eliche-Moral et al. 2010a,b; Robaina et al. 2010; Oesch et al. 2010).

Hence, we need other mechanisms than major mergers to transform intermediate-mass blue cloud galaxies into red sequence ones. One possible mechanism is minor merging. The N -body simulations find that minor mergers increase the Sérsic index of galaxies (Eliche-Moral et al. 2006) and that several minor mergers have the same effect as a major one: only the final mass accreted is important (i.e., ten 1/10 mergers are equivalent to one equal-mass merger, Bournaud et al. 2007). We find that the minor-to-major merger ratio of blue galaxies increases between $z = 0.8$ and $z = 0.5$ from ~ 0.5 to ~ 2 , indicating that minor mergers may play an important role in the growth of the red sequence since $z \sim 0.5$. However, we find that the mass accreted by minor mergers is $\sim 15\%$ of the mass accreted by major mergers at $z = 0.8$, and ~ 0.6 at $z = 0.5$. Even in the lower redshift range, where minor mergers are twice more common than major ones in blue galaxies, the latter are more efficient in transforming gas-rich galaxies into E/S0. In addition, the observed $R_{\text{mm}}^{\text{blue}}$ implies that, in the range $[0.2, 0.95]$, a gas-rich galaxy have only undergone $N_{\text{mm}}^{\text{blue}} \sim 0.15$ minor mergers, making it unlikely that a gas-rich galaxy suffers more than one minor merger since $z \sim 1$. In summary, our observations indicate that minor mergers affect less the structure of gas-rich galaxies than major mergers

in the redshift range under study, and they can lead into early spirals instead of into E/S0.

It is also expected that secular processes can transform late spirals into early ones. Bars and disk instabilities support the growth of the central part of the galaxies, called pseudo-bulges (Kormendy & Kennicutt 2004; Fisher et al. 2009). The similar disc and nuclear colours of spirals up to $z \sim 0.8$ (Domínguez-Palmero & Balcells 2008) also points towards a co-ordinated growth of the bulge and the disc, while Masters et al. (2011), and Sheth et al. (2008) and Cameron et al. (2010) find that early-type spirals have higher bar fractions than late-type ones in Galaxy Zoo ($z \sim 0.04$), and COSMOS⁶ ($0.2 < z < 0.85$), respectively. The comparison of the observational (this paper, López-Sanjuan et al. 2010a) and theoretical (Oesch et al. 2010) major + minor merger rate against the number density growth of intermediate-mass, early-type galaxies also suggests that secular processes are needed.

If these early, bulge-dominated systems, whatever their origin, have their star formation shut down by some processes unrelated to mergers, as gas exhaustion (Zheng et al. 2007; Bauermeister et al. 2010) or some form of quenching (e.g., morphological quenching, Martig et al. 2009; or environment quenching, Peng et al. 2010), they then become passive early-type disc on the red sequence, as those found by Bundy et al. (2010).

It is also worth noting that because the merger fraction increases when μ decreases, it is possible that galaxies smaller / fainter than studied in this paper may play a significant role. However, we find that the increase in the merger fraction cannot compensate for the decrease in the mass of the companion and the increase in the typical merger timescale, so it is not expected that mergers with $\mu < 1/10$ have been important in the evolution of intermediate-mass gas-rich galaxies. Cosmological models also suggest that merger events lower than $\mu < 1/10$ have little impact (less than 10%) in the mass assembly of spheroids (Hopkins et al. 2010a).

8. Summary and conclusions

We have estimated, for the first time in the literature, the minor merger fraction and rate of $L_B \gtrsim L_B^*$ galaxies from kinematically confirmed close pairs, reaching the minor companion regime, $1/10 \leq \mu < 1/4$ ($\Delta M_B = 1.5 - 2.5$) thanks to the deep spectroscopy in VVDS-Deep ($I_{\text{AB}} \leq 24$), and robust statistics in a wide 0.5 deg^2 area.

We find that minor mergers for bright galaxies show little evolution with redshift as a power-law $(1 + z)^m$ with index $m = -0.4 \pm 0.7$ for the merger fraction and $m = -0.5 \pm 0.7$ for the merger rate, while the major merger fraction ($m = 1.3 \pm 0.5$) and rate ($m = 1.3 \pm 0.6$) for the same galaxies increases. The dependence of the merger fraction on μ is well described by a power-law function, $f_m(\geq \mu) \propto \mu^s$. The value of s for the complete magnitude-limited sample, $M_B^{\text{e}} \leq -20$, evolves from $s = -0.60 \pm 0.08$ at $z = 0.8$ to $s = -1.02 \pm 0.13$ at $z = 0.5$. When we split our bright galaxies in red and blue following the rest-colour bimodality, we find that in the redshift range explored i) f_m is higher for red galaxies at every μ , ii) f_m^{red} does not evolve with z , with $s = -0.79 \pm 0.12$ at $0.2 < z < 0.95$, and iii) f_m^{blue} evolves dramatically: the major merger fraction of blue galaxies decreases by a factor of three with cosmic time, while the minor merger fraction of blue galaxies is roughly constant.

⁶ Cosmological Evolution Survey, Scoville et al. 2007 (<http://cosmos.astro.caltech.edu/index.html>).

Our results show that normal $L_B \gtrsim L_B^*$ galaxies have undergone 0.4 minor and 0.4 major mergers since $z \sim 1$, which implies a total mass growth from major and minor mergers with $\mu \geq 1/10$ by about 25%. The relative contribution of the mass growth by merging is $\sim 25\%$ due to minor mergers with $1/10 \leq \mu < 1/4$ and $\sim 75\%$ due to major mergers with $\mu \geq 1/4$. The relative effect of merging is more important for red than for blue galaxies, with red galaxies subject to 0.5 minor and 0.7 major mergers since $z \sim 1$. This leads to a mass growth of $\sim 40\%$ and a size increase by a factor of 2 of red galaxies, in agreement with the evolution of massive galaxies as reported by previous works (e.g., van der Wel 2008; van Dokkum et al. 2010). This supports that mergers are an important contributor to the evolution of the most massive red galaxies since $z \sim 1$. For blue galaxies, our results imply that minor mergers likely lead to early-type spirals rather than elliptical galaxies.

Our analysis therefore shows that minor merging is a significant but not dominant mechanism contributing to the mass growth of galaxies in the last ~ 8 Gyr. Merging alone is not sufficient to explain the observed mass growth of galaxies, and other processes must therefore be operating. The contribution from minor merging of low mass companions with $\mu < 1/10$ is yet to be estimated, but we expect that this contribution would have only limited effects.

To expand on our observational results, the study of the minor merger fraction in other fields will be needed to minimize cosmic variance effect, on larger samples to better constrain the evolution of f_{mm} with redshift. In addition, the study of the dependence of minor mergers on properties like mass, morphology or environment will provide other important clues about the role of mergers in the evolution of galaxies since $z \sim 1$. It is also worth noting that direct measurements of the minor merger fraction have yet to be secured at low redshift, while these will be needed to better constrain the minor merger fraction evolution with z .

Acknowledgements. We dedicate this paper to the memory of our six IAC colleagues and friends who met with a fatal accident in Piedra de los Cochinos, Tenerife, in February 2007, with a special thanks to Maurizio Panniello, whose teachings of python were so important for this paper.

We thank the anonymous referee for his/her comments and suggestions, that improved the quality of the paper.

C. L. S. acknowledge the funding support of ANR-07-BLAN-0228 and the help of A. Ealet in the statistical analysis.

A. P. has been supported by the research grant of the Polish Ministry of Science Nr N N203 51 29 38 and the European Associated Laboratory "Astrophysics Poland-France".

This work uses the Millennium Galaxy Catalogue, which consists of imaging data from the Isaac Newton Telescope and spectroscopic data from the Anglo Australian Telescope, the ANU 2.3m, the ESO New Technology Telescope, the Telescopio Nazionale Galileo, and the Gemini North Telescope. This survey was supported through grants from the Particle Physics and Astronomy Research Council (UK) and the Australian Research Council (AUS). The data and data products of this survey are publicly available from <http://www.eso.org/~jliske/mgc/> or on request from J. Liske or S.P. Driver.

References

Abbas, U., de La Torre, S., Le Fèvre, O., et al. 2010, MNRAS, 406, 1306
 Adelman-McCarthy, J. K., Agüeros, M. A., Allam, S. S., et al. 2006, ApJS, 162, 38
 Aitken, A. C. 1935, Proc. R. Soc. Edinb, 55, 42
 Arnouts, S., Walcher, C. J., Le Fèvre, O., et al. 2007, A&A, 476, 137
 Bauermeister, A., Blitz, L., & Ma, C. 2010, ApJ, 717, 323
 Bell, E. F., Phleps, S., Somerville, R. S., et al. 2006, ApJ, 652, 270
 Bezanson, R., van Dokkum, P. G., Tal, T., et al. 2009, ApJ, 697, 1290
 Bournaud, F., Jog, C. J., & Combes, F. 2007, A&A, 476, 1179
 Brammer, G. B., Whitaker, K. E., van Dokkum, P. G., et al. 2009, ApJ, 706, L173
 Bridge, C. R., Carlberg, R. G., & Sullivan, M. 2010, ApJ, 709, 1067
 Brown, M. J. I., Dey, A., Jannuzi, B. T., et al. 2007, ApJ, 654, 858
 Brown, M. J. I., Zheng, Z., White, M., et al. 2008, ApJ, 682, 937
 Buitrago, F., Trujillo, I., Conselice, C. J., et al. 2008, ApJ, 687, L61
 Bundy, K., Ellis, R. S., & Conselice, C. J. 2005, ApJ, 625, 621
 Bundy, K., Fukugita, M., Ellis, R. S., et al. 2009, ApJ, 697, 1369
 Bundy, K., Scarlata, C., Carollo, C. M., et al. 2010, ApJ, 719, 1969
 Cameron, E. 2010, PASA, submitted [ArXiv:1012.0566]
 Cameron, E., Carollo, C. M., Oesch, P., et al. 2010, MNRAS, 409, 346
 Conselice, C. J. 2006, ApJ, 638, 686
 Conselice, C. J., Bershady, M. A., Dickinson, M., & Papovich, C. 2003, AJ, 126, 1183
 Conselice, C. J., Bundy, K., Trujillo, I., et al. 2007, MNRAS, 381, 962
 Conselice, C. J., Yang, C., & Bluck, A. F. L. 2009, MNRAS, 361
 Cool, R. J., Eisenstein, D. J., Fan, X., et al. 2008, ApJ, 682, 919
 Cortese, L., Boselli, A., Franzetti, P., et al. 2008, MNRAS, 386, 1157
 Cox, T. J., Jonsson, P., Primack, J. R., & Somerville, R. S. 2006, MNRAS, 373, 1013
 Cox, T. J., Primack, J., Jonsson, P., & Somerville, R. S. 2004, ApJ, 607, L87
 Cucciati, O., Marinoni, C., Iovino, A., et al. 2010, A&A, 520, A42+
 Daddi, E., Renzini, A., Pirzkal, N., et al. 2005, ApJ, 626, 680
 Darg, D. W., Kaviraj, S., Lintott, C. J., et al. 2010, MNRAS, 401, 1043
 De Propris, R., Conselice, C. J., Liske, J., et al. 2007, ApJ, 666, 212
 De Propris, R., Liske, J., Driver, S. P., Allen, P. D., & Cross, N. J. G. 2005, AJ, 130, 1516
 de Ravel, L., Le Fèvre, O., Tresse, L., et al. 2009, A&A, 498, 379
 Domínguez-Palmero, L. & Balcells, M. 2008, A&A, 489, 1003
 Driver, S. P., Liske, J., Cross, N. J. G., De Propris, R., & Allen, P. D. 2005, MNRAS, 360, 81
 Drory, N. & Alvarez, M. 2008, ApJ, 680, 41
 Drory, N., Salvato, M., Gabasch, A., et al. 2005, ApJ, 619, L131
 Efron, B. 1982
 Eliche-Moral, M. C., Balcells, M., Aguerri, J. A. L., & González-García, A. C. 2006, A&A, 457, 91
 Eliche-Moral, M. C., Prieto, M., Gallego, J., et al. 2010a, A&A, 519, A55
 Eliche-Moral, M. C., Prieto, M., Gallego, J., & Zamorano, J. 2010b, ApJ, submitted [ArXiv: 1003.0686]
 Ellison, S. L., Patton, D. R., Simard, L., & McConnachie, A. W. 2008, AJ, 135, 1877
 Faber, S. M., Willmer, C. N. A., Wolf, C., et al. 2007, ApJ, 665, 265
 Fernández-Ontiveros, J. A., López-Sanjuan, C., Montes, M., Prieto, M. A., & Acosta-Pulido, J. A. 2011, MNRAS, 411, L21
 Fisher, D. B., Drory, N., & Fabricius, M. H. 2009, ApJ, 697, 630
 Fontana, A., Santini, P., Grazian, A., et al. 2009, A&A, 501, 15
 Franzetti, P., Scoglio, M., Garilli, B., et al. 2007, A&A, 465, 711
 Genel, S., Bouché, N., Naab, T., Sternberg, A., & Genzel, R. 2010, ApJ, 719, 229
 Giallongo, E., Salimbeni, S., Menci, N., et al. 2005, ApJ, 622, 116
 González-García, A. C., Oñorbe, J., Domínguez-Tenreiro, R., & Gómez-Flechoso, M. Á. 2009, A&A, 497, 35
 Hopkins, P. F., Bundy, K., Croton, D., et al. 2010a, ApJ, 715, 202
 Hopkins, P. F., Bundy, K., Hernquist, L., Wuyts, S., & Cox, T. J. 2010b, MNRAS, 401, 1099
 Hopkins, P. F., Bundy, K., Murray, N., et al. 2009a, MNRAS, 398, 898
 Hopkins, P. F., Cox, T. J., Younger, J. D., & Hernquist, L. 2009b, ApJ, 691, 1168
 Hopkins, P. F., Hernquist, L., Cox, T. J., Dutta, S. N., & Rothberg, B. 2008, ApJ, 679, 156
 Hopkins, P. F., Somerville, R. S., Cox, T. J., et al. 2009c, MNRAS, 397, 802
 Ilbert, O., Arnouts, S., McCracken, H. J., et al. 2006, A&A, 457, 841
 Ilbert, O., Salvato, M., Le Floc'h, E., et al. 2010, ApJ, 709, 644
 Ilbert, O., Tresse, L., Zucca, E., et al. 2005, A&A, 439, 863
 Jaech, J. L. 1964, JASA, 59, 863
 Jiang, C. Y., Jing, Y. P., Faltenbacher, A., Lin, W. P., & Li, C. 2008, ApJ
 Jogee, S., Miller, S. H., Penner, K., et al. 2009, ApJ, 697, 1971
 Kaviraj, S., Khochfar, S., Schawinski, K., et al. 2008, MNRAS, 388, 67
 Kaviraj, S., Peirani, S., Khochfar, S., Silk, J., & Kay, S. 2009, MNRAS, 394, 1713
 Kaviraj, S., Schawinski, K., Devriendt, J. E. G., et al. 2007, ApJS, 173, 619
 Kaviraj, S., Tan, K., Ellis, R. S., & Silk, J. 2011, MNRAS, in press [ArXiv: 1001.2141]
 Kitzbichler, M. G. & White, S. D. M. 2008, MNRAS, 1300
 Kormendy, J. & Kennicutt, Jr., R. C. 2004, ARA&A, 42, 603
 Le Fèvre, O., Abraham, R., Lilly, S. J., et al. 2000, MNRAS, 311, 565
 Le Fèvre, O., Guzzo, L., Meneux, B., et al. 2005a, A&A, 439, 877
 Le Fèvre, O., Mellier, Y., McCracken, H. J., et al. 2004, A&A, 417, 839
 Le Fèvre, O., Saisse, M., Mancini, D., et al. 2003, in Society of Photo-Optical Instrumentation Engineers (SPIE) Conference Series, Vol. 4841, Society of Photo-Optical Instrumentation Engineers (SPIE) Conference Series, ed.

M. Iye & A. F. M. Moorwood, 1670–1681

Le Fèvre, O., Vettolani, G., Garilli, B., et al. 2005b, A&A, 439, 845

Lin, L., Cooper, M. C., Jian, H., et al. 2010, ApJ, 718, 1158

Lin, L., Koo, D. C., Willmer, C. N. A., et al. 2004, ApJ, 617, L9

Lin, L., Patton, D. R., Koo, D. C., et al. 2008, ApJ, 681, 232

Lintott, C. J., Schawinski, K., Slosar, A., et al. 2008, MNRAS, 389, 1179

Liske, J., Lemon, D. J., Driver, S. P., Cross, N. J. G., & Couch, W. J. 2003, MNRAS, 344, 307

López-Sanjuan, C., Balcells, M., García-Dabó, C. E., et al. 2009a, ApJ, 694, 643

López-Sanjuan, C., Balcells, M., Pérez-González, P. G., et al. 2010a, A&A, 518, A20+

López-Sanjuan, C., Balcells, M., Pérez-González, P. G., et al. 2009b, A&A, 501, 505

López-Sanjuan, C., Balcells, M., Pérez-González, P. G., et al. 2010b, ApJ, 710, 1170

Lotz, J. M., Davis, M., Faber, S. M., et al. 2008, ApJ, 672, 177

Lotz, J. M., Jonsson, P., Cox, T. J., & Primack, J. R. 2010a, MNRAS, 404, 590

Lotz, J. M., Jonsson, P., Cox, T. J., & Primack, J. R. 2010b, MNRAS, 404, 575

Maller, A. H., Katz, N., Kereš, D., Davé, R., & Weinberg, D. H. 2006, ApJ, 647, 763

Martig, M., Bournaud, F., Teyssier, R., & Dekel, A. 2009, ApJ, 707, 250

Masters, K. L., Nichol, R. C., Hoyle, B., et al. 2011, MNRAS, in press [ArXiv: 1003.0449]

McCracken, H. J., Radovich, M., Bertin, E., et al. 2003, A&A, 410, 17

Mihos, J. C. & Hernquist, L. 1994, ApJ, 425, L13

Naab, T., Jesseit, R., & Burkert, A. 2006, MNRAS, 372, 839

Naab, T., Johansson, P. H., & Ostriker, J. P. 2009, ApJ, 699, L178

Oesch, P. A., Carollo, C. M., Feldmann, R., et al. 2010, ApJ, 714, L47

Patton, D. R. & Atfield, J. E. 2008, ApJ, 685, 235

Patton, D. R., Carlberg, R. G., Marzke, R. O., et al. 2000, ApJ, 536, 153

Patton, D. R., Ellison, S. L., Simard, L., McConnachie, A. W., & Mendel, J. T. 2011, MNRAS, 14

Patton, D. R., Pritchett, C. J., Carlberg, R. G., et al. 2002, ApJ, 565, 208

Peng, Y., Lilly, S. J., Kováč, K., et al. 2010, ApJ, 721, 193

Pozzetti, L., Bolzonella, M., Lamareille, F., et al. 2007, A&A, 474, 443

Pozzetti, L., Bolzonella, M., Zucca, E., et al. 2010, A&A, 523, A13+

Rawat, A., Hammer, F., Kembhavi, A. K., & Flores, H. 2008, ApJ, 681, 1089

Robaina, A. R., Bell, E. F., van der Wel, A., et al. 2010, ApJ, 719, 844

Roseboom, I. G., Pimbblet, K. A., Drinkwater, M. J., et al. 2006, MNRAS, 373, 349

Rothberg, B. & Fischer, J. 2010, ApJ, 712, 318

Rothberg, B. & Joseph, R. D. 2006a, AJ, 131, 185

Rothberg, B. & Joseph, R. D. 2006b, AJ, 132, 976

Salim, S., Dickinson, M., Michael Rich, R., et al. 2009, ApJ, 700, 161

Scarlata, C., Carollo, C. M., Lilly, S. J., et al. 2007, ApJS, 172, 494

Schiminovich, D., Wyder, T. K., Martin, D. C., et al. 2007, ApJS, 173, 315

Scodellaggio, M., Franzetti, P., Garilli, B., et al. 2005, PASP, 117, 1284

Scoville, N., Aussel, H., Brusa, M., et al. 2007, ApJS, 172, 1

Sheth, K., Elmegreen, D. M., Elmegreen, B. G., et al. 2008, ApJ, 675, 1141

Springel, V., White, S. D. M., Jenkins, A., et al. 2005, Nature, 435, 629

Stewart, K. R., Bullock, J. S., Wechsler, R. H., & Maller, A. H. 2009, ApJ, 702, 307

Taylor, E. N., Franx, M., Glazebrook, K., et al. 2010, ApJ, 720, 723

Toft, S., Franx, M., van Dokkum, P., et al. 2009, ApJ, 705, 255

Trujillo, I., Cenarro, A. J., de Lorenzo-Cáceres, A., et al. 2009, ApJ, 692, L118

Trujillo, I., Conselice, C. J., Bundy, K., et al. 2007, MNRAS, 382, 109

Trujillo, I., Förster Schreiber, N. M., Rudnick, G., et al. 2006, ApJ, 650, 18

van der Wel, A. 2008, ApJ, 675, L13

van der Wel, A., Holden, B. P., Zirm, A. W., et al. 2008, ApJ, 688, 48

van Dokkum, P. G., Franx, M., Kriek, M., et al. 2008, ApJ, 677, L5

van Dokkum, P. G., Whitaker, K. E., Brammer, G., et al. 2010, ApJ, 709, 1018

Vergani, D., Scodellaggio, M., Pozzetti, L., et al. 2008, A&A, 487, 89

Walcher, C. J., Lamareille, F., Vergani, D., et al. 2008, A&A, 491, 713

Wild, V., Walcher, C. J., Johansson, P. H., et al. 2009, MNRAS, 395, 144

Williams, R. J., Quadri, R. F., Franx, M., van Dokkum, P., & Labbé, I. 2009, ApJ, 691, 1879

Williams, R. J., Quadri, R. F., Franx, M., et al. 2010, ApJ, 713, 738

Woods, D. F. & Geller, M. J. 2007, AJ, 134, 527

Wyder, T. K., Martin, D. C., Schiminovich, D., et al. 2007, ApJS, 173, 293

Zheng, X. Z., Bell, E. F., Papovich, C., et al. 2007, ApJ, 661, L41

Zucca, E., Bardelli, S., Bolzonella, M., et al. 2009, A&A, 508, 1217

Zucca, E., Ilbert, O., Bardelli, S., et al. 2006, A&A, 455, 879

² Institute for Astronomy, University of Edinburgh, Blackford Hill, Edinburgh EH9 3HJ, U.K.

³ INAF-Osservatorio Astronomico di Bologna, Via Ranzani 1, I-40127, Bologna, Italy

⁴ Laboratoire d’Astrophysique de Toulouse-Tarbes, Université de Toulouse, CNRS, 14 av. E. Belin, F-31400 France

⁵ IASF-INAF, Via Bassini 15, I-20133, Milano, Italy

⁶ INAF-Osservatorio Astronomico di Brera, Via Brera 28, I-20021, Milan, Italy

⁷ Institut d’Astrophysique de Paris, UMR 7095, 98 bis Bd Arago, F-75014, Paris, France

⁸ Observatoire de Paris, LERMA, 61 Avenue de l’Observatoire, F-75014, Paris, France

⁹ The Andrzej Soltan Institute for Nuclear Studies, ul. Hoza 69, 00-681 Warszawa, Poland

¹⁰ Astronomical Observatory of the Jagiellonian University, ul Orla 171, PL-30-244, Kraków, Poland

¹¹ Center for Theoretical Physics PAS, Al. Lotników 32/46, 02-668 Warsaw, Poland

Appendix A: Merger fraction fitting by Generalized Least Squares

The dependence of the merger fraction $f_m (\geq \mu)$ with μ is well described by a power-law function (Eq. [7]). However, our definition of f_m is cumulative, so the points in Tables 1, 5 and 6 are not independent and their errors are correlated. To obtain reliable fit parameters and their uncertainties we used the Generalized Least Squares (GLS; Aitken 1935) method, which takes into account not only the variance of the data, but also the covariance between them. For a given r_p^{\max} and redshift range, we followed the next steps to estimate the covariance matrix of the data:

1. We extracted a random point, named $f_m^{\text{sim}} (\mu \geq 1/2)$, as drawn for a Gaussian distribution with mean $f_m (\mu \geq 1/2)$ and standard deviation $\sigma_{f_m} (\mu \geq 1/2)$. In this process we imposed that the random point had to be positive, i.e., negative merger fractions are nonphysical.
2. To obtain the next merger fraction, named $f_m^{\text{sim}} (\mu \geq 1/3)$, we extracted a random point as drawn for a Gaussian with mean $f_m (\mu \geq 1/3) - f_m (\mu \geq 1/2)$ and standard deviation $[\sigma_{f_m}^2 (\mu \geq 1/3) - \sigma_{f_m}^2 (\mu \geq 1/2)]^{1/2}$, and added it to the previous $f_m^{\text{sim}} (\mu > 1/2)$. In this process we set a negative random point to zero, that is, we imposed that merger fractions are cumulative when μ decreases. In addition, this process takes into account that the errors are correlated.
3. We repeated the step 2 for all the μ values under study down to $\mu = 1/10$. This provided us a set of $f_m^{\text{sim}} (\geq \mu)$.
4. We repeated 100000 times the steps 1 – 3 and estimated the covariance matrix of the observational merger fractions using the simulated ones.

We checked that our simulated merger fractions are a good description of the observational ones. We found that all the distributions of $f_m^{\text{sim}} (\geq \mu)$ are well described by a Gaussian, as desired. In Fig. A.1 we show the observational and the simulated merger fractions for $r_p^{\max} = 100 h^{-1}$ kpc at $z_{r,2}$ and for $r_p^{\max} = 30 h^{-1}$ kpc at $z_{r,1}$. We choose these two examples because they are the best and the worst simulated cases, respectively. Observational and simulated merger fractions are in agreement in the first case, but in the second case the values of the merger fraction are slightly overestimated (less than 5%), while the standard deviations are underestimated (less than 10%). To understand the origin of this discrepancy, we studied the distribution of $f_m^{\text{sim}} (\mu \geq 1/10)$ for both cases, Fig. A.2. In the first case the

¹ Laboratoire d’Astrophysique de Marseille, Pôle de l’Etoile Site de Château-Gombert 38, rue Frédéric Joliot-Curie, F-13388 Marseille, France

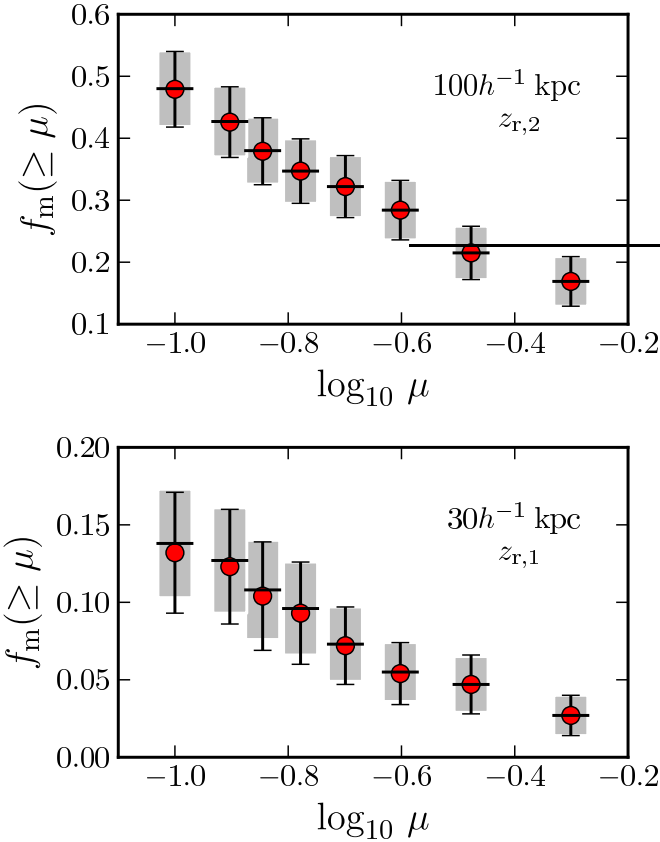


Fig. A.1. Merger fraction as a function of $\log_{10} \mu$. We use these particular axis to facilitate the visualization. The dots and the error bars are the observational data. The gray areas are the 1σ confidence intervals of the simulated merger fractions, while the horizontal black lines are their mean (see text for details). *Top panel:* Merger fraction for $r_p^{\max} = 100h^{-1}$ kpc at $z_{r,2}$. *Bottom panel:* Merger fraction for $r_p^{\max} = 30h^{-1}$ kpc at $z_{r,1}$. [A colour version of this plot is available at the electronic edition].

simulated distribution and that expected from observations are in excellent agreement. However, in the second case we find less points than expected at low values of the merger fraction. This is due to the lower values of the observed merger fraction at $z_{r,1}$ and the higher errors for $r_p^{\max} = 30h^{-1}$ kpc measurements. This leads to negative random points, which we did not take into account (step 1) or set to zero (step 2), so we missed simulated values in the lower tail of the distribution. Despite of that, the global simulated distribution is a good description of the expected one: if we only use the upper tail of the distribution to describe it, the difference between the observed and the simulated values of the merger fraction and its standard deviation becomes lower than 2% and 3%, respectively. Hence, we conclude that the simulated merger fractions describe well the observational ones and that the estimated covariance matrix is a good approximation to the real one.

Using the covariance matrix, we applied the GLS to estimate f_{MM} and s (Eq. [7]). We noted that the errors in f_{MM} are similar or higher than the errors in the observed major merger fractions, so we can not obtain new information of f_{MM} from the GLS analysis. Hence, we set the value of f_{MM} to the observed one and used GLS to estimate the power-law index s . To obtain reliable fits given the cumulative nature of the data, we opted to use the $\mu = 1/10$ (lower μ value), $\mu = 1/4$ (the fixed major

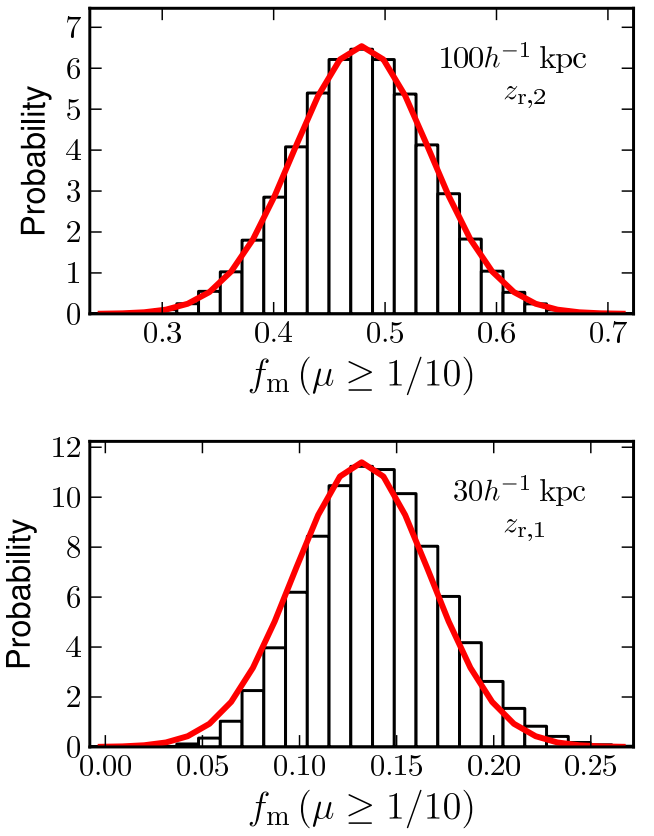


Fig. A.2. Probability distributions of the simulated merger fractions for $\mu > 1/10$ and $r_p^{\max} = 100h^{-1}$ at $z_{r,2}$ (*upper*), and for $r_p^{\max} = 30h^{-1}$ at $z_{r,1}$ (*lower*). The solid line is not a fit to the histogram, but the expected distribution from the observational merger fraction. [A colour version of this plot is available at the electronic edition].

merger fraction) and $\mu = 1/2$ (higher μ value) data points, as we noticed that, as expected, most of the slope information is contained in these three points (Jaech 1964). This produces a stable fit at every r_p^{\max} , as shown in Fig. A.3 for $50h^{-1}$ kpc separations. Adding other 5 intermediate points is only decreasing the variance on s by 10-15% but is producing low quality fits as shown in Fig. A.3 (i.e., the fitted curves depart more than 1σ from the observational data), which is traced to the increase in observational errors: analytically all the information is contained in a few μ points and the GLS does not take into account most of the data in the fit.

In summary, all the power-law index s quoted in the paper were obtained from a GLS fit to $\mu = 1/10, 1/4$ and $1/2$ merger fraction data, and using simulated merger fractions to estimate their covariance matrix.

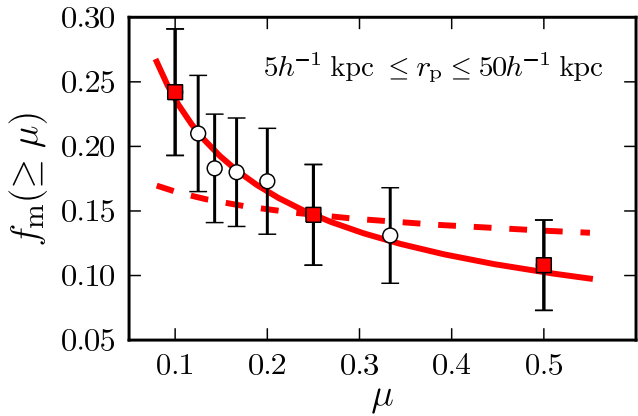


Fig. A.3. Generalized Least Squares fit to all the data (dashed line) and to the squares ($\mu = 1/10, 1/4$ and $1/2$; solid line). Observed merger fractions are for $r_p^{\max} = 50h^{-1}$ kpc at $z_{r,2}$. [A colour version of this plot is available at the electronic edition].